Dissertations, Theses, and Masters Projects   Theses, Dissertations, & Master Projects

1999

Analysis of Mercury Coordination Environments of Tridentate and Tetradentate Imidazole Based Ligands by X-Ray Crystallography and NMR Spectroscopy

Geoffrey Murphy
College of William & Mary - Arts & Sciences

Follow this and additional works at: https://scholarworks.wm.edu/etd

Part of the Analytical Chemistry Commons

Analysis of Mercury Coordination Environments of Tridentate and

Tetradentate Imidazole Based Ligands by X-ray Crystallography and

NMR Spectroscopy

A Thesis

Presented to

The Faculty of the Department of Chemistry

The College of William & Mary in Virginia

In Partial Fulfillment

Of the Requirements for the Degree of

Master of Arts

by
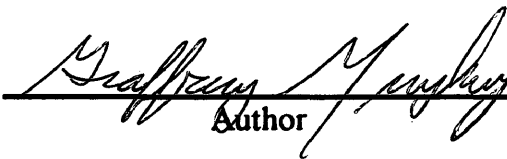
Geoffrey Murphy

1999

Approval Sheet

This thesis is submitted in partial fulfillment

of the requirements for the degree of

Master of Arts

(signature)
Author

Approved, July 1999

(signature)
Deborah C. Bebout

(signature)
Richard L. Kiefer
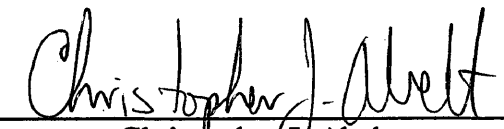
(signature)
Christopher J. Abelt

Table of Contents

ACKNOWLEDGEMENTS

I would like to especially thank Dr. Bebout for her patience, guidance and encouragement throughout this project. In addition the research performed by previous students, whose work provided a foundation for this study. I would also like to thank the other members of the laboratory group, especially Christine and Janice, for providing assistance and support the past year. A special thanks to the chemistry graduate students for their constant encouragement. Finally, I would like to thank my family and friends whose support has helped motivate this accomplishment.

LIST OF TABLES

LIST OF FIGURES

ABSTRACT

The effects of mercury(II) coordination by the potentially tridentate ligand bis(2-(1-methylimidazolyl)methyl)amine (B-MIMA) and potentially tetradentate ligand bis((2-pyridyl)methyl)((1-methylimiazol-2-yl)methyl)amine (BPIA) were studied by X-ray crystallography and solution-state NMR. Deuterated acetonitrile solutions containing metal-to-ligand ratios of 0 to 2.0 were examined. Mercury coordinated complexes were characterized exhibiting $^1H^{199}Hg$ coupling at low temperature in the solution-state. Solid-state structures obtained by X-ray crystallography were correlated with the NMR data. The eight-coordinate complex $[Hg(BPIA)_2](ClO_4)_2$ crystallizes in the monoclinic space group c2/c with a = 21.4151(18) Å, b = 11.8611(10) Å, c = 17.6893(15) Å, α = 90°, β = 96.467(7)°, γ = 90° with Z = 4. This complex is tetradentate with a Hg-N_{amine} distance of 2.829 Å, Hg-$N_{pyridyl}$ distances of 2.884 Å and 2.702 Å and a Hg-$N_{imidazole}$ distance of 2.159(5) Å. The complex exhibits an inversion center through the mercury(II) ion of a bicapped trigonal antiprism. The five-coordinate complex $[Hg(B-MIMA)Cl_2]$ crystallizes in the monoclinic space group $P2_1/c$ with a = 12.055(3) Å, b = 8.9660(9) Å, c = 13.5517(14) Å, α = 90°, β = 98.827(18)°, γ = 90° with Z = 4. This complex is tridentate with a Hg-N_{amine} distance of 2.640(6) Å and an average Hg-$N_{imidazole}$ distance of 2.272(8) Å. The complex exhibits a metal coordination sphere of a distorted trigonal bipyramid.

Analysis of Mercury Coordination Environments of Tridentate and

Tetradentate Imidazole Based Ligands by X-ray Crystallography and

NMR Spectroscopy

INTRODUCTION

There are few physiological processes that do not require protein function and interaction.[1] The chemical reactions which sustain life would not be possible under physiological conditions without the presence of enzymes, which are protein catalysts. Protein functions range from the transport of energy in photosynthesis and respiration to antibody defense of organisms against foreign invasion. Proteins function as structural elements in cells and as regulators of gene expression. Despite the diversity in protein function, proteins are composed of different combinations of the same 20 amino acids. Only the number and sequence of these 20 amino acids differentiates between proteins.

Over 30 years ago, Anfinsen demonstrated that the final three-dimensional shape of a native protein was determined by the linear amino acid sequence.[2] This three-dimensional shape of the native protein is required for the protein to become completely biologically active. An error within the native protein structure or a problem with the protein folding mechanism often leads to severe physiological complications within an organism.[3] Several types of interactions properly stabilize the native structure of a protein. These stabilizing features include interactions between amino acids, both in the same chain and on different protein chains, hydrophobic and hydrophilic interactions with the protein's environment, and interactions with molecules not initially associated with the protein. The stabilization of the protein by a metal cofactor is an example of this last type of interaction.

2

An estimated 30-50% of all proteins require metal interactions for complete physiological activity.[4] These metal ions may facilitate protein folding or be directly involved with the chemistry at the active site of a protein. Metal ion binding sites are created by the cooperative interaction of ligating protein groups, which leads to metal specificity. It is hypothesized that metal ions may be involved in the thermodynamic stabilization of protein folding intermediates. Experiments have demonstrated that the rate of protein folding can be slowed by up to three orders of magnitude in the presence of metal chelators.[5] Characterization of the metal coordination environment of a protein is crucial to fully understanding the role of the metal in protein function.

There are a variety of analytical techniques currently available to characterize protein sequences and structures.[1] The sequence of small proteins can be determined from Edman degradation and Sangar sequencing of complementary DNA. Mass spectrometric techniques have also been developed for determination of protein sequences. Circular dichroism (CD) can be used to determine the relative amounts of α-helical, β-sheet, and random coiled conformations present. Infrared spectroscopy can also approximate the amounts of secondary protein structure present. The size of a protein can be determined through sedimentation analysis, gel filtration, or SDS polyacrylamide gel electrophoresis. Unfortunately, none of these techniques provide specific information about the three-dimensional structure of a protein. The only techniques that can provided detailed three-dimensional protein structures are X-ray diffraction analysis and nuclear magnetic resonance spectroscopy.

X-ray diffraction requires a single crystal of the protein for structure elucidation. Successful interpretation of the protein structure by X-ray crystallography requires large,

well-ordered crystals with each protein molecule held in a specific position within the crystal lattice.[1] Unfortunately, proteins have irregular surfaces which can impede crystallization. Furthermore, while X-ray crystallography can provide the specific structure of a protein, this method cannot provide information about the kinetics of metal ion incorporation into a protein. Since this information is crucial to understanding the folding mechanism of proteins, another analytical technique is required for analysis. Nuclear magnetic resonance spectroscopy (NMR) allows for proteins to be studied in solution and is thus a valuable complement to X-ray crystallography.

Nuclei with spin are required for NMR.[6] Isotopes with an odd molecular weight, or an odd number of protons and neutrons, are capable of having spin. The spinning motion of a charged nucleus creates a magnetic field. When this tiny magnet is exposed to an external magnetic field of larger magnitude, the spin vector is either aligned with the magnetic field or against it. Alignment with the external field is more energetically favorable for the nucleus. These two possibilities are designated as spin states and there is a slight excess of nuclei population in the lower energy spin state in accordance with the Boltzmann distribution.

The spin states of a nucleus provide the necessary conditions for spectroscopy. By applying an energy source that matches the difference in frequency between the spin states, resonance occurs. The energy source disturbs the equilibrium between the spin states, enhancing the population of the less energetically favorable state. After excitation, the spins relax, returning to the more favorable state. The energy difference between the two spin states is directly related to the strength of the external magnetic field. The larger the external field strength, the greater the energy difference.

Spin coupling in NMR provides important information about the environment of a particular nucleus.[7] This phenomenon manifests itself in a spectra as split NMR peaks and occurs when there is indirect coupling of nuclear spins through the intervening bonding electrons. As a result, the nucleus resonates at two or more slightly different frequencies because it can experience two slightly different magnetic environments. The frequency difference between these two environments is proportional to the effectiveness of the coupling and is denoted by the spin coupling constant, J. This constant is independent of the applied magnetic field and usually only slightly affected by a change in solvent. The magnitude of J depends upon the type and number of bonds through which the nuclei are coupled. There is a casual relationship between coupling constants and dihedral bond angles using the Karplus relationship. However, many other factors other than dihedral angles influence coupling constants.

Optimization of parameters can enhance the effectiveness of NMR as an analytical tool. Proton NMR is used on proteins frequently because protons are an abundant, sensitive nucleus. Unfortunately, protons have a very limited chemical shift range, which leads to considerable spectral overlap when studying proteins. Since many proteins incorporate metal ions into their native structure, including their active sites, NMR characterization of these metal-binding sites can provide valuable insight. Nuclei with spin states $I = \frac{1}{2}$ are favorable because the peaks are fairly narrow and internuclear coupling can be readily resolved. The nuclei should also possess a large natural abundance and a wide chemical shift range. Biologically relevant spin $I = \frac{1}{2}$ nuclei include ^1H, ^{13}C, ^{15}N and ^{113}Cd. The natural abundance of these nuclei range from very low (^{13}C, 1.1%) to very high (^1H, 99.9%). The chemical shift ranges also vary among

these nuclei. One metal ion which possesses favorable NMR characteristics is ^{199}Hg. ^{199}Hg has a natural abundance of 16.85% and a receptivity 5.4 times greater than ^{13}C.[8] In addition, the chemical shift of ^{199}Hg, a chemical shift range of about 5000 ppm, is very sensitive to the number and identity of bound nuclei.

Unfortunately, none of the physiologically relevant metals possess nuclei with favorable NMR properties. The most common physiological metals include zinc, copper, iron and magnesium. The transition metals iron, zinc and copper tend to bind imidazole nitrogens of histidine residues and the sulfur atoms of cysteine and methionine. Magnesium ions are commonly bound by the carboxylate and phosphate groups of proteins. One important class of metalloproteins is the zinc finger proteins.[1] This class of proteins binds specifically to DNA and thus are of great biological importance because they are generally involved in replication or expression of genetic information. The zinc-finger proteins possess the ability to bind to specific sequences of DNA. The unique structural feature of the zinc finger proteins is a Zn^{2+} ion chealted by two cystein and two histidine residues. These four residues are placed in their approximate positions by folding of the apo-polypeptide, but the zinc ion further stabilizes the three-dimensional structure.

While NMR can provide information about protein structure, it usually does not adequately characterize metal-protein interactions due to large protein size and the presence of NMR inactive nuclei. The most detailed structural information about protein metal-binding sites comes from X-ray crystal structures. The Extended X-ray Absorption Fine Structure (EXAFS) technique can also be used to determine the type, number and distances of atoms coordinating the metal ion. However, both X-ray crystallography and

EXAFS are unable to monitor the protein in solution and its folding/unfolding mechanism. Since none of these techniques routinely provide a complete picture of the metal binding site of proteins in solution, there is considerable motivation to develop a novel NMR metalloprobe which would allow for the study of metal coordination site of proteins in solution.

One of the first metals used as a NMR probe of proteins was ^{113}Cd substituted for native zinc in proteins.[9,10] This technique has provided substantial information about the metal binding sites of these proteins, including types of coordinating groups and conformational changes. Studies have demonstrated trends between ^{113}Cd chemical shifts and structural features of metal ion binding sites in proteins. Recently, mercury substitution of metal ions within proteins has been demonstrated to have similar capabilities and occur with minor structural differences.[11-13]

Two examples of mercury substituted proteins include poplar plastocyanin and *P. Furiosus* rubredoxin. Only modest differences were found between the crystal structures of mercury-substituted plastocyanin, a native copper(II) protein.[11] Due to the larger size of the mercury atom, there was a slight enlargement of the coordination polyhedron. Also, mercury possesses a greater affinity for sulfur ligands, so the substituted protein showed a smaller bond length to the sulfur atom. In *P. Furiosus* rubredoxin, it was shown by NMR that protons far from the metal center were unaffected by substitution of mercury for zinc.[12]

Other examples of mercury substituted proteins include *P. aeruginosa* azurin and spinach plastocyanin.[13] It was originally believed that the large anisotropies expected for mercury-protein environments would broaden the ^{199}Hg line widths. Utschig *et al.*

demonstrated with azurin and spinach plastocyanin that spectra can be obtained in reasonable time with reasonable line widths relative to the ^{199}Hg chemical shift range at high field strength. They also showed that the ^{199}Hg chemical shifts are sensitive to subtle variations in the coordination chemistry of proteins with copper sites. For example, the mercury-substituted azurin was found to have a 135 ppm ^{199}Hg shift upfield relative to the mercury-substituted plastocyanin. This upfield shift is consistent with a different coordination environment that leads to greater shielding in the azurin. Using ^{113}Cd, the shift difference was only 60 ppm demonstrating the greater sensitivity of ^{199}Hg chemical shifts in metalloprotein coordination environments.

Another ^{199}Hg NMR technique which may provide even more information is the heteronuclear multiple quantum coherence (HMQC) method. Heteronuclear coupling is used in this technique to identify the protons of amino acid side chains which are directly associated with an NMR active metal. The coupled ^{1}H and ^{199}Hg signals in a two-dimensional HMQC spectra allow for correlation with their chemical shifts. Blake et al. have observed weak correlation signals in P. furiosus rubredoxin for protons separated from the metal by four bonds.[12] Weak scalar coupling of protons to the mercury that were separated by a minimum of six covalent bonds were also observed. The proposed theory is that an overlap of orbitals of the proton and metal-coordinated sulfur atom caused a "through-space" interaction mechanism. These "through-space" interactions may be useful in determining the three-dimensional conformation of metalloproteins.

These examples and techniques demonstrate that ^{199}Hg NMR is and will be a powerful tool in elucidating the three-dimensional structure of metalloproteins. However, a thorough chemical shift data library of complexes of known structure is

needed. This information will allow for ^{199}Hg NMR to be used to obtain structural information about novel mercury complexes. One reason such a data library has remained undeveloped is due to the instability of mercuric complexes in solution. In this study, a family of multidentate imidazoyl ligands, which model the active sites of metalloproteins which contain histidine, were developed. These small organic molecules are much easier to study via NMR than are actual proteins due to the fact that proteins contain many NMR-active nuclei. The steric constraints of these ligands are meant to provide a model of protein metal binding site structure.

Previous ^{199}Hg NMR studies focused on using several monodentate ligands, which proved difficult due to the rapid exchange of these small ligands.[14] To decrease these exchange problems, ligands with higher coordination numbers are used here. In this study, both a tridentate and tetradentate ligand have been synthesized. These bulkier ligands provide a model of protein active sites due to their greater geometric constraints. The two ligands synthesized (Figure 1) and investigated were bis(2-(1-methylimidazolyl)methyl)amine (B-MIMA) and bis((2-pyridyl)methyl)((1-methylimiazol-2-yl)methyl)amine (BPIA).
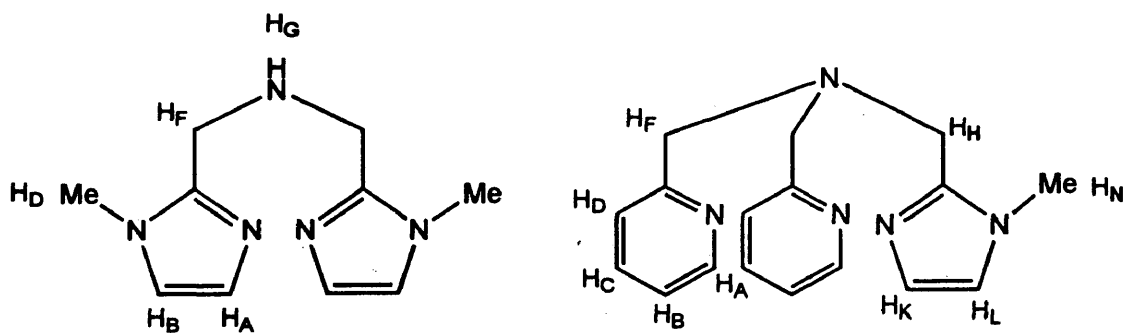

Figure 1. B-MIMA and BPIA

B-MIMA, a tridentate ligand, acts as a model of a protein active site containing three nitrogen residues. The ligand contains two imidazoyl rings which are used to simulate the amino acid histidine. The two imidazoyl rings are connected to a secondary amine via methylene bridges. Methyl groups are present on one of the nitrogens in the imidazoyl rings to decrease the number of resonance structures. This methyl protecting group also keeps the nitrogen atom it is bound to from coordinating with a metal ion. B-MIMA could potentially be used to simulate active sites with coordination numbers of three or six.

Oberhausen *et al.* have used B-MIMA to form complexes with a copper ion.[15] They were able to obtain X-ray quality crystals of the copper complex [Cu(B-MIMA)(CH$_3$COO$^-$)](ClO$_4$), which has a four coordinate geometry around the metal ion. This four coordinate geometry results from the bonding of three nitrogen atoms from B-MIMA and an oxygen atom from the acetate ion. This group also observed solution spectroscopic properties for the complex which suggested that the solid state square-pyramidal geometry of the metal ion is not retained in the solution state.

BPIA, a tetradentate ligand, models a protein active site containing four nitrogen residues. The ligand contains two pyridyl rings and one imidazole ring, which attach to a tertiary amine via methylene bridges. The aromatic heterocycles simulates the amino acid histidine.. The imidazoyl ring has the methyl group connected to one of its nitrogens as in B-MIMA. BPIA can potentially be used to simulate active sites with coordination numbers of four or eight.

Previous studies have used BPIA in coordination studies with a copper ion. Wei *et al.* were able to obtain X-ray quality crystals of [(BPIA)$_2$Cu$_2$](CF$_3$SO$_3$)$_2$.[16] A four

coordinate geometry around the metal ion was observed which resulted from the bonding of four nitrogen atoms from BPIA. The geometry about each copper ion is distorted trigonal pyramidal. Oberhausen *et al.* were also able to obtain the compound [Cu(BPIA)(1-MeIm)](PF$_6$)$_2$, but have not yet obtained X-ray quality crystals.[17]

The need for understanding the metal-binding site of metalloproteins is crucial to completely understanding protein folding/unfolding mechanisms. A relatively new technique used to study the active site of metalloproteins is [199]Hg NMR. Substituting mercury into proteins may provide insight into the determination of unknown metal-binding sites. By synthesizing small organic molecules to mimic the active site environment, a chemical shift data library may be created for [199]Hg NMR. This library would allow for a greater understanding of proteins, which are vital to almost all biological processes. In this study two organic ligands were synthesized and coordinated with mercury(II). Both of these ligands contain imidazoyl rings which mimic the amino acid histidine. By studying both the solution state NMR and crystal structure of mercury(II) coordination complexes of these ligands, it is hoped that more information will be made available to further develop [199]Hg NMR as a metalloprobe.

EXPERIMENTAL

All reagents and solvents used were of commercially available reagent quality unless otherwise noted. All syntheses were performed under argon, except for X-ray crystal growth, and organic products and crystals were purged with argon for storage. The purity of all intermediate compounds was checked by ^{1}H NMR. The purity of ligands was confirmed by ^{1}H and ^{13}C NMR and IR spectroscopy. Melting points were obtained using a Mel-Temp® melting point apparatus. Infrared spectra were taken in KBr pellets on a Nicolet 20DXB Fourier Transform Infrared Spectrophotometer. Atlantic Microlabs, Inc., of Norcross, Georgia conducted elemental analyses.

Nuclear Magnetic Resonance Spectroscopy was performed on all room temperature samples using a Varian 400 MHz spectrometer. Low temperature NMR runs were performed on a General Electric QE-300 Multinuclear NMR spectrometer, with a variable temperature (VT) unit. The VT unit held sample temperatures constant at -40° C by immersing the air coils into liquid nitrogen and blowing cold, dry nitrogen over the sample in the probe. Chemical shifts are reported relative to tetramethylsilane.

Single crystal X-ray diffraction data were obtained in collaboration with Raymond J. Butcher at Howard University. Data were collected at 20° C on a Siemens P4S four-circle diffractometer using a graphite-monochromated Mo Kα X-radiation (λ = 0.71073 Å) and the θ-2θ technique over a 2θ range of 3-55°. During data collection three standard reflections were measured after every 97 reflections. Crystals turned black in

the beam. The structures were solved by direct methods and Fourier difference maps using the SHELXTL-PLUS[18] package of software programs. Final refinements were done using SHELXL-93[19] minimizing $R2 = [\Sigma[w(F_o^2 - F_c^2)^2]/\Sigma[w(F_o^2)^2]]^{1/2}$, $R1 = \Sigma| |F_o| - |F_c| |/\Sigma|F_o|$, and $S = [\Sigma[w(F_o^2 - F_c^2)^2]/(n - p)]^{1/2}$. All non-hydrogen atoms were refined as anisotropic and the hydrogen atomic positions were fixed relative to the bonded carbons and the isotropic thermal parameters were fixed.

All of the perchlorate salts of mercury(II) complexes included in this work were stable for routine synthesis and purification procedures. However, caution should be exercised because perchlorate salts of metal complexes with organic ligands are potentially explosive.[20]

Synthesis of 1-methyl-2-imidazolecarboxaldehyde (MICA)

This procedure was adapted from Oberhausen et al.[15] In a round bottom flask, a suspension of 1-methylimidazole (16.0 mL, 0.20 mol) was made in 500 mL of dry diethyl ether. The flask was lowered into a dry ice/acetone bath to bring the temperature to −50 °C. The 1-methylimidazole crystallized out of the solution at this temperature. To the cold solution, 1.6 M n-butyllithium (140 mL, 0.216 mol) was added. Caution must be used when working with the n-butyllithium since it cannot be exposed to air or moisture. This solution was allowed to mix for approximately two hours at −50 °C after which dimethylformamide (25 mL, 0.30 mol) in 40 mL of dry diethyl ether was quickly added. The solution was stirred at −50 °C for another hour and then stirred at 4 °C overnight in a refrigerator. Over a period of 10 minutes, 25 mL of water was added to the solution. This was followed by 130 mL of 4 M hydrochloric acid. The acid layer was collected and the ether washed 5 more times with 30 mL portions of 4 M hydrochloric acid. The

acid extracts were combined and saturated with potassium carbonate. This solution was extracted with 4 x 120 mL chloroform. The chloroform extracts were combined, dried over magnesium sulfate, and filtered. The solution was concentrated *in vacuo* to yield a yellow oil as the product. The yellow oil was distilled at reduced pressure to give 14 g (64% yield) of a colorless product that crystallized upon standing. **Mp:** 36-38 °C [1]**H** **NMR:** (DMSO-d_6) (Appendix 1) δ 3.38 (s, 3H), 3.93 (water), 7.24 (s, 1H), 7.57 (s, 1H), 9.68 (s, 1H).

Synthesis of 1-methyl-2-imidazolecarboxaldehyde oxime (MICAO)

This procedure was adapted from Oberhausen *et al.*[15] Hydroxylamine hydrochloride (19.0 g, 0.273 mol) and sodium carbonate (14.5 g, 0.1365 mol) were dissolved in 20 ml of water cooled to 0 °C. To this solution 1-methyl-2-imidazolecarboxaldehyde (28.0 g, 0.255 mol) in 10 ml of ethanol was added. A precipitate formed in the reaction vessel. The solution was refluxed for 3 hours and then allowed to crystallize overnight at 4 °C in a refrigerator. The precipitate was filtered and washed with 30 ml of cold 33% ethanol to give 30.7 g (97% yield) of a white solid. **Mp:** 168-170 °C [1]**H NMR:** (DMSO-d_6) (Appendix 2) δ 3.82 (s, 3H), 7.00 (s, 1H), 7.27 (s, 1H), 8.07 (s, 1H).

Synthesis of 1-methyl-2-aminomethylimidazole dihydrochloride (MAMI)

This procedure was adapted from Oberhausen *et al.*[15] A solution of 1-methyl-2-imidazolecarboxaldehyde oxime (5.0 g, 0.04 mol) in 250 ml of methanolic hydrochloride was hydrogenated at 45 psi and room temperature over 10% palladium-carbon for 3 hours. A white product formed in the hydrogenation jar and it was necessary to heat the

solution to dissolve the product before filtering the catalyst through a bed of Celite. The catalyst was washed with 25 ml of methanol and the filtrate cooled to −20 °C overnight. The precipitate was filtered and washed with 4 x 10 ml portions of methanolic hydrochloride to give 3.5 g (50% yield) of light brown solid. The filtrate was then concentrated *in vacuo* and placed again at −20 °C overnight. A second crop of product was obtained (0.5 g to 2.0 g). The procedure was repeated as necessary to gain maximum yield of the product (57 − 79% yield). **Mp:** 248-250 °C **^{1}H NMR:** (DMSO-d$_6$) (Appendix 3) δ 3.15 (water), 3.95 (s, 3H), 4.42 (s, 2H), 7.75 (s, 1H), 7.76 (s, 1H), 9.25 (bs, 2H).

Synthesis of bis(2-(1-methylimidazolyl)methyl)amine trihydrochloride (B-MIMA • 3HCl)

This procedure was adapted from Oberhausen *et al.*[15] In 200 mL of methanol, 1-methyl-2-aminomethylimidazole dihydrochloride (8.0 g, 0.044 mol) was dissolved along with potassium hydroxide (5.0 g, 0.088 mol). The 1-methylimidazolecarboxaldehyde (5.0 g, 0.044 mol) was dissolved in 50 mL of methanol and then added to the solution. The solution was hydrogenated for four hours at 10 psi over 10% palladium-carbon. When finished, the solution was filtered through a bed of Celite and rinsed with methanol to remove the catalyst. The filtrate was concentrated *in vacuo* to approximately 75 mL. The solution was filtered to remove any precipitated salt and then 60 mL of methanoic hydrochloride was added. The mixture was placed into a freezer for precipitation of 3.5 g (25.8% yield) of greenish, flaky crystals. **Mp:** 210-212 °C **^{1}H NMR:** (DMSO-d$_6$) δ 3.16 (water), 3.95 (s, 3H), 4.53 (s, 2H), 5.12 (bs, 4H), 7.71 (s, 1H), 7.77 (s, 1H). (Spectrum not shown since alternate synthesis of B-MIMA had higher yield).

Synthesis of bis(2-(1-methylimidazolyl)methyl)amine (B-MIMA) Method 1

This procedure was adapted from Oberhausen *et al.*[15] The bis(2-(1-methylimidazolyl)methyl)amine trihydrochloride (10.0 g, 0.032 mol) was dissolved in an aqueous solution of sodium bicarbonate (5.37g, 0.064 mol). The solution was allowed to stir at room temperature for approximately fifteen minutes and then extracted with (5 X 50 mL) chloroform. The chloroform was removed under reduced pressure giving a small amount of yellow oil, which crystallized upon standing to give 2.0 g (30% yield) of B-MIMA. Mp: 118-120 °C ^{1}H NMR: (acetonitrile-d_3) (Appendix 4) δ 2.09 (s, 1H), 3.54 (s, 6H), 3.73 (s, 4H), 6.79 (s, 2H), 6.91 (s, 2H). ^{13}C NMR: δ 33.008, 45.445, 122.371, 127.504, 147.474 IR: (Appendix 10)

Synthesis of bis(2-(1-methylimidazolyl)methyl)amine (B-MIMA) Method 2

This procedure was adapted from Morgenstern-Badarov *et al.*[21] 1-Methylimidazolecarboxaldehyde oxime (6.5g, 0.05 mol) was dissolved in 200 mL of methanol. The solution was hydrogenated at less than 1 psi H_2 over 10% palladium-carbon for five days. After five days the solution was filtered through a bed of Celite and the catalyst rinsed with 15 mL of methanol. The filtrate was concentrated under reduced pressure to give 5.3 g of a colorless oil. To this oil was added 1.5 mL of ethyl acetate and the mixture placed into a freezer for precipitation. The precipitate was filtered and rinsed with ethyl acetate to give 4.2 g (82% yield) of a white, crystalline solid. Mp: 118-120 °C ^{1}H NMR: (acetonitrile-d_3) (Appendix 4) δ 2.09 (s, 1H), 3.54 (s, 6H), 3.73 (s, 4H), 6.79 (s, 2H), 6.91 (s, 2H). ^{13}C NMR: δ 33.008, 45.445, 122.371, 127.504, 147.474 IR: (Appendix 10)

Synthesis of 2-(hydroxymethyl)-1-methylimidazole (HMMI)

The following procedure was adapted from Wei, *et al.*[16] 1-Methylimidazole (79.75 mL, 1.0 mol) and paraformaldehyde (60.0 g, 2.0 mol) were dissolved in 200 mL of distilled water and refluxed for four days. The mixture was removed from heat and allowed to cool to room temperature before concentrating *in vacuo*. The concentrated solution was extracted with methylene chloride (5 x 100 mL). The organic portions were collected and dried over magnesium sulfate, filtered, and solvent removed under reduced pressure to produce a clear, viscous oil. The oil was placed into the freezer giving 26.07 (23.3% yield) of a white, crystalline material. Mp: 109-111 °C. ^{1}H NMR: (DMSO-d_6) (Appendix 5) : δ 3.36 (s, 3H), 3.63 (water), 4.46 (s, 2H), 5.25 (bs, 1H), 6.75 (s, 1H), 7.05 (s, 1H).

Synthesis of 2-(chloromethyl)-1-methylimidazole hydrochloride (CMMI)

The following procedure was adapted from Wei *et al.*[16] A solution of 2-(hydroxymethyl)-1-methylimidazole (25.0 g, 0.223 mol) dissolved in 100 mL of chloroform was added dropwise to a solution of thionyl chloride (110 mL) and chloroform (320 mL), which had been cooled to 0 °C in an ice bath. After dropwise addition, the reaction mixture was removed from the ice bath and allowed to warm to room temperature before refluxing for two hours. After refluxing, the solvent was removed under reduced pressure to dryness. The resulting solid was suspended in diethyl ether and stirred overnight. The off-white solid was collected via vacuum filtration to give 22.3 g (91% yield) . Mp: 174-176 °C ^{1}H NMR: (DMSO-d_6) (Appendix 6) δ 3.88 (s, 3H), 5.19 (s, 2H), 7.70 (s, 1H), 7.78 (s, 1H).

Synthesis of (bis((2-pyridyl)methyl)((1-methylimidazolyl)methyl)amine) (BPIA)

The following procedure was adapted from Wei et al.[16] 2-(Chloromethyl)-1-methylimidazole (4.94 g, 0.038 mol) was suspended in 100 mL of methylene chloride and the mixture cooled to 0 °C in an ice bath. To this mixture, bis((2-pyridyl)methyl)amine (6.81 mL, 0.038 mol) in 15 mL of methylene chloride was slowly added. This was followed by the addition of triethylamine (10.54 mL, 0.76 mol) in 30 mL of methylene chloride. The reaction mixture was allowed to stir at 0 °C for approximately fifteen minutes and then allowed to warm to room temperature. After stirring at room temperature for two days the solution was washed with water (2 x 200 mL) and 2 M sodium hydroxide solution (1 x 100 mL). The organic phase was then dried over magnesium sulfate, treated with activated charcoal, and then filtered. The resulting solution was concentrated under reduced pressure to give a dark brown oil which crystallized from diethyl ether to give 5.1 g (61% yield) of a slightly off-white solid. **Mp:** 88-89 °C **^{1}H NMR:** (DMSO-d_6) (Appendix 7) δ 3.35 (water), 3.49 (s, 3H), 3.70 (s, 2H), 3.72 (s, 4H), 6.74 (s, 1H), 7.02 (s, 1H), 7.25 (dd, 2H, J =), 7.45 (d, 2H, J=), 7.75 (t, 2H, J=), 8.49 (d, 2H, J=). **^{13}C NMR:** 33.332, 51.264, 60.807, 122.762, 123.024, 124.242 (2) 127.562, 137.246, 149.884, 160.260 **IR:** (Appendix 11)

Synthesis of [Hg(BPIA)$_2$](ClO$_4$)$_2$ • toluene

BPIA (200 mg, 0.68 mmol) was dissolved in 3 mL of acetonitrile. To this was added a 2 mL solution containing Hg(ClO$_4$)$_2$ • 3H$_2$O (156 mg, 0.34 mmol). To this solution 1.2 mL of toluene was added to make a 80/20 acetonitrile:toluene solution. The solution was split into two separate vials, loosely capped, and allowed to stand for slow evaporation of the solvent. After several days, there were many colorless, X-ray quality

. crystals. **Mp:** 89-90 °C ^{1}**H NMR:** (acetonitrile-d_3) (Appendix 8) δ 2.33 (s, water), 3.60 (s, 6H), 4.07 (s, 2H), 4.11 (s, 4H), 5.74 (s, 1H), 6.78 (s, 1H), 7.05 (dd, 2H), 7.20 (m, 2H), 7.44 (d, 2H), 7.77 (t, 2H)   **IR:**   (Appendix 12) **Elemental Anaylsis of** $C_{41}H_{46}N_{10}Cl_2O_8Hg$: Calc. C, 45.7% ; H, 4.27% ; N, 13.0%. Found C, 45.49% ; H, 4.27% ; N, 13.0%.

Synthesis of [Hg(B-MIMA)Cl₂]

B-MIMA (100 mg, 0.49 mmol) was dissolved in 6 mL of acetonitrile. To this was added a 6 mL solution containing HgCl₂ (133 mg, 0.49 mmol) dissolved in acetonitrile. To this solution 4 mL of toluene was added to make a 75/25 acetonitrile:toluene solution. The solution was allowed to stand in a beaker with a watch glass over top of it. Several crystals formed within twenty minutes , but all had solvent trapped inside. The mother liquor was allowed to stand and approximately one hour later, there were many colorless, X-ray quality crystals. **Mp:** 195-200 °C ^{1}**H NMR:** (acetonitrile-d_3) (Appendix 9) δ 2.14 (s, 1H), 3.57 (s, 3H), 3.97 (s, 2H), 7.02 (s, 1H), 7.08 (s, 1H)   **IR:** (Appendix 13)   **Elemental Analysis of** $C_{10}H_{15}N_5Cl_2Hg$: Calc. C, 25.3% ; H, 3.2% ; N, 14.7%. Found: C, 25.36% ; H, 3.08% ; N, 14.52%.

X-ray Crystallography of [Hg(BPIA)₂](ClO₄)₂ • toluene

A crystal measuring 0.10 x 0.68 x 0.16 mm was glued to the end of a glass fiber. No decay of the intensity was observed and no absorption correction was performed on these data. Ψ scans showed significant variation and an empirical absorption correction was applied to the data. The final data-to-parameter ratio was 15:1.

X-ray Crystallography of [Hg(B-MIMA)Cl₂]

A crystal measuring 0.17 x 0.47 x 0.37 mm was glued to the end of a glass fiber. No decay of the intensity was observed and no absorption correction was performed on these data. Ψ scans showed significant variation and the SHELXA absorption correction was applied to the data. The final data-to-parameter ratio was 18:1.

RESULTS AND DISCUSSION

I. ORGANIC SYNTHESES

The synthesis of B-MIMA, via method 1, required the synthesis of several intermediate products. The first of these products, 1-methyl-2-imidazolecarboxaldehyde (MICA), was synthesized from commercially available starting materials, via a 3-step addition reaction. In the first step, 1-methylimidazole had its most acidic proton stripped by n-butyllithium to form a carbanion. The second step involved the carbanion attacking the carbonyl of dimethylformamide to from a tetrahedral intermediate. The final step produced the desired product MICA and dimethylamine. Purification of the crude product was achieved via vacuum distillation.
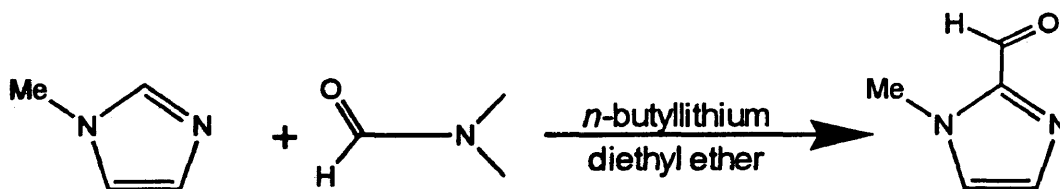
Figure 2. Synthesis of 1-methyl-2-imidazolecarboxaldehyde (MICA)

A condensation reaction between MICA and hydroxylamine with loss of water generated 1-methyl-2-imidazolecarboxaldehyde oxime (MICAO). Sodium carbonate neutralized the hydrochloric acid released by hydroxylamine hydrochloride. Vacuum filtration and rinsing with ethanol provided product of adequate purity.
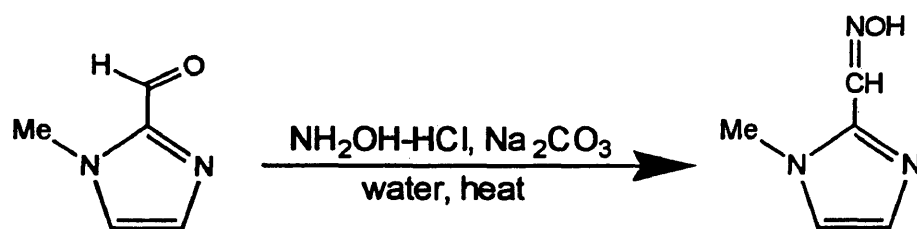
Figure 3. Synthesis of 1-methyl-2-imidazolecarboxaldehyde oxime (MICAO)

The third intermediate, 1-methyl-2-aminomethylimidazole dihydrochloride, was synthesized via a reductive amination reaction. MICAO was reduced via catalytic hydrogenation using palladium on carbon in methanolic hydrochloride. After removal of the catalyst, the product crystallized from the chilled filtrate.
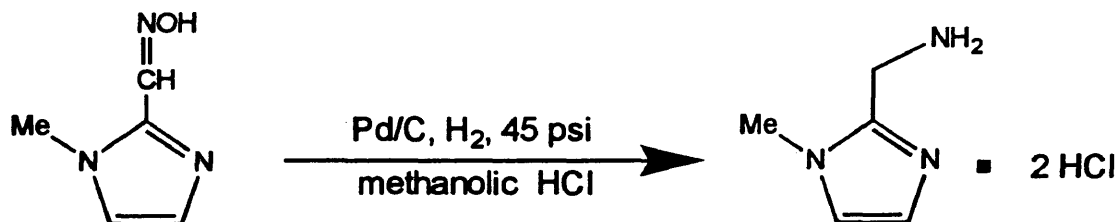

Figure 4. Synthesis of 1-methyl-2-aminomethylimidazole dihydrochloride (MAMI)

Bis(2-(1-methylimidazolyl)methyl)amine trihydrochloride (B-MIMA • 3HCl), the final intermediate was produced by another reductive amination reaction. Potassium hydroxide was used to generate the free base of MAMI. The amine attacked the carbonyl of MICA. This reaction was accompanied with the loss of water and formation of a double bond. This intermediate species was reduced via catalytic hydrogenation using palladium on carbon. Purified product was vacuum filtered and rinsed clean.

22
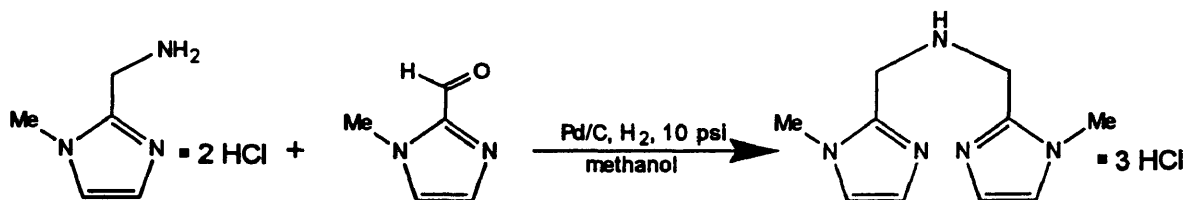
Figure 5. Synthesis of bis(2-(1-methylimidazolyl)methyl)amine trihydrochloride
(B-MIMA • 3HCl)

Method 1 for the synthesis of the tridentate ligand bis(2-(1-methylimidazolyl)methyl)amine (B-MIMA), was completed by neutralizing B-MIMA • 3HCl to a free base. Potassium carbonate was used to liberate the hydrochlorides and B-MIMA was purified via recrystallization with ethyl acetate.
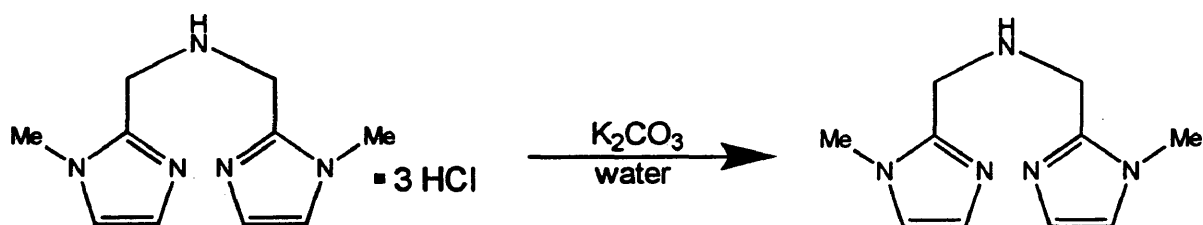

Figure 6. Synthesis of bis(2-(1-methylimidazolyl)methyl)amine (B-MIMA)

The synthesis of B-MIMA via method 2 proved to be much simpler and produced the desired product in better yields. MICAO was catalytically hydrogenated for five days using palladium on carbon and low H_2 pressure. During this hydrogenation the free base of MAMI was produced, which then reacted with MICAO, releasing hydroxyamine, to give B-MIMA. The product was purified via recrystallization with ethyl acetate.
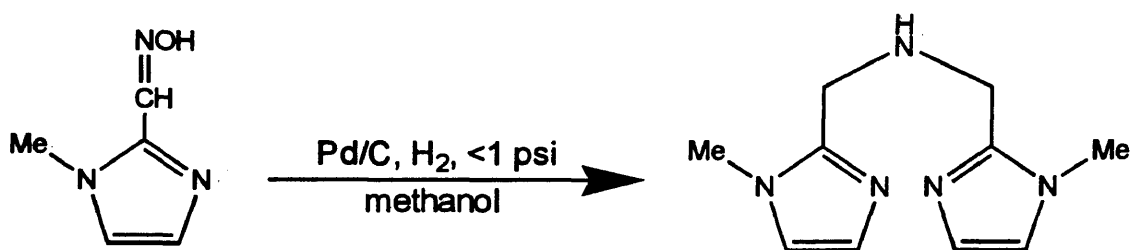
Figure 7. Method 2 for synthesis of bis(2-(1-methylimidazolyl)methyl)amine
(B-MIMA)

The synthesis of (bis((2-pyridyl)methyl)((1-methylimidazol-2-yl)methyl)amine) (BPIA) only required two intermediates produced. The first of these, 2-(hydroxymethyl)-1-methylimidazole (HMMI), was synthesized via electrophilic aromatic substitution. Formaldehyde, released from paraformaldehyde, acted as the electrophile forming a tetrahedral intermediate at the carbon with the most acidic hydrogen. This reaction provided substantially lower yields than those reported in the literature. The product was recovered via vacuum filtration.
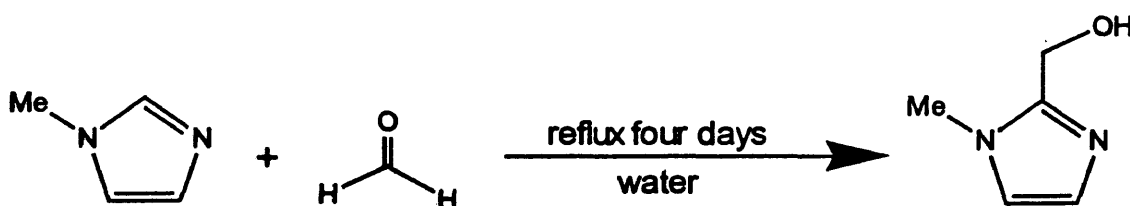
Figure 8. Synthesis of 2-(hydroxymethyl)-1-methylimidazole (HMMI)

The second compound required for BPIA synthesis, 2-(chloromethyl)-1-methylimidazole hydrochloride, was formed via a two-step substitution mechanism. In the first step, an alkyl chlorosulfate was formed using HMMI and thionyl chloride. In the second step, a S$_N$2 displacement occured producing the desired product in good yields. The crude product obtained by rotary evaporation of the reaction mixture and the solid

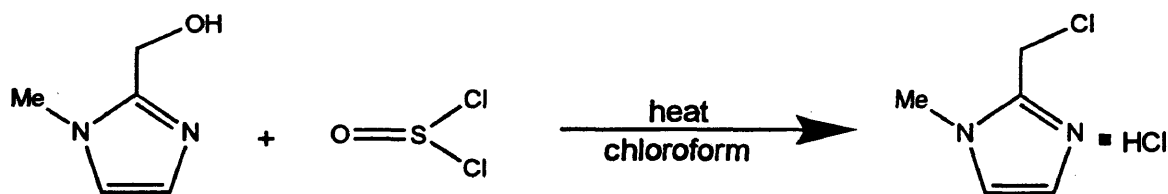obtained was triturated with diethyl ether. The final product was recovered by vacuum filtration.

Figure 9. Synthesis of 2-(chloromethyl)-1-methylimidazole hydrochloride (CMMI)

BPIA was synthesized via nucleophilic alkylation. Bis(2-pyridylmethyl)amine (BMPA), obtained commercially, attacked CMMI releasing hydrochloric acid and yielding the tertiary amine product. The HCl was neutralized with triethylamine and the final product crystallized from diethyl ether.
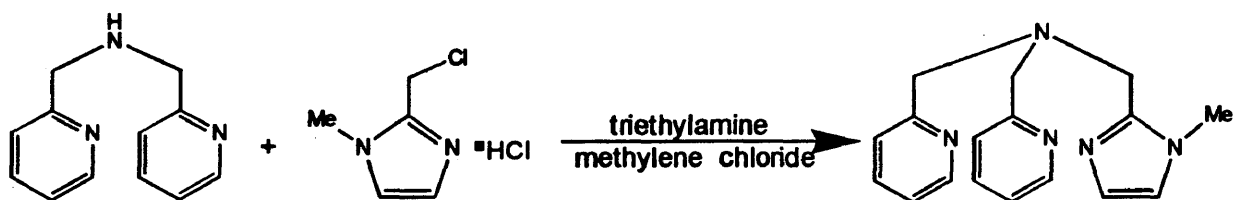

Figure 10. Synthesis of (bis((2-pyridyl)methyl)((1-methylimidazol-2-yl)methyl)amine (BPIA)

25

II. X-RAY DIFFRACTION ANALYSIS STUDIES

Crystal Structure of [Hg(BPIA)$_2$](ClO$_4$)$_2$ • toluene

This complex was made by slow evaporation from acetonitrile/toluene using a 1:2 ratio of mercury perchlorate to BPIA. A thermal ellipsoid diagram of the cation complex is given in Figure 11, a unit cell diagram in Figure 12, general crystallographic information is summarized in Table 1, selected bond lengths are given in Table 2, and selected bond angles are given in Table 3.

This complex is eight-coordinate, and all donor nitrogens are part of two chelating organic ligands. The two ligands are related by inversion about the mercury center. The Hg-N$_{amine}$ and Hg-N$_{pyridyl}$ bond distances are very similar averaging 2.805 Å. The Hg-N$_{imidazole}$ bond distance of 2.159(5) Å is noticeably shorter. The Hg-N$_{pyridyl}$ bond distances in this complex are also longer than similar bonds observed in [Hg(pyridine)$_6$](CF$_3$SO$_3$)$_2$.[22]

The only metal complex involving BPIA reported previously is [(BPIA)$_2$Cu$_2$](CF$_3$SO$_3$)$_2$.[17] In this dinuclear complex, the two BPIA molecules are coordinated with both copper(I) atoms. Each four coordinate copper(I) atom is bound to the amine and two pyridyl groups of one BPIA molecule and to the imidazole nitrogen from the second BPIA molecule. All of the metal-nitrogen bond distances are noticeably shorter in the copper(I) complex compared to the mercury(II) complex. Also the average Cu-N$_{pyridyl}$ bond distance of 2.123(13) Å is closer to the Cu-N$_{imidazole}$ distance of 1.941(8) Å.

The mercury(II) complex of BPIA can be compared more directly to the eight coordinate complex [Hg(TMPA)$_2$](ClO$_4$)$_2$ (TMPA=tris[(2-pyridyl)methyl]amine).[23] Both

complexes exhibit an inversion center through the mercury(II) ion of a bicapped trigonal antiprism, but the bond distances are strikingly different. The Hg-N_{amine} bond distance for TMPA is 2.560(3) Å, while it is 2.829 Å for BPIA. TMPA also has one pyridyl ring which is more tightly bound than the other two rings. This pyridyl ring can be compared with the imidazoyl ring of BPIA. The average Hg-$N_{pyridyl}$ bond distance for the two rings of TMPA that are not as tightly bound is 2.594(7) Å which is much shorter than the 2.793 Å average Hg-$N_{pyridyl}$ bond distance for the BPIA complex. The pyridyl ring, which occupies a similar position to the imidazoyl ring of BPIA, has a Hg-$N_{pyridyl}$ bond distance of 2.562(3) Å while the Hg-$N_{imidazole}$ bond distance is 2.159(5) Å. This comparison to TMPA may indicate that since the imidazoyl nitrogen is more tightly coordinated to the mercury ion, the pyridyl rings of BPIA are pushed out away from the metal center in order to adopt a stable conformation. Clearly the data presented demonstrates that a novel environment for the mercury ion has been formed using BPIA molecules as coordinating ligands.
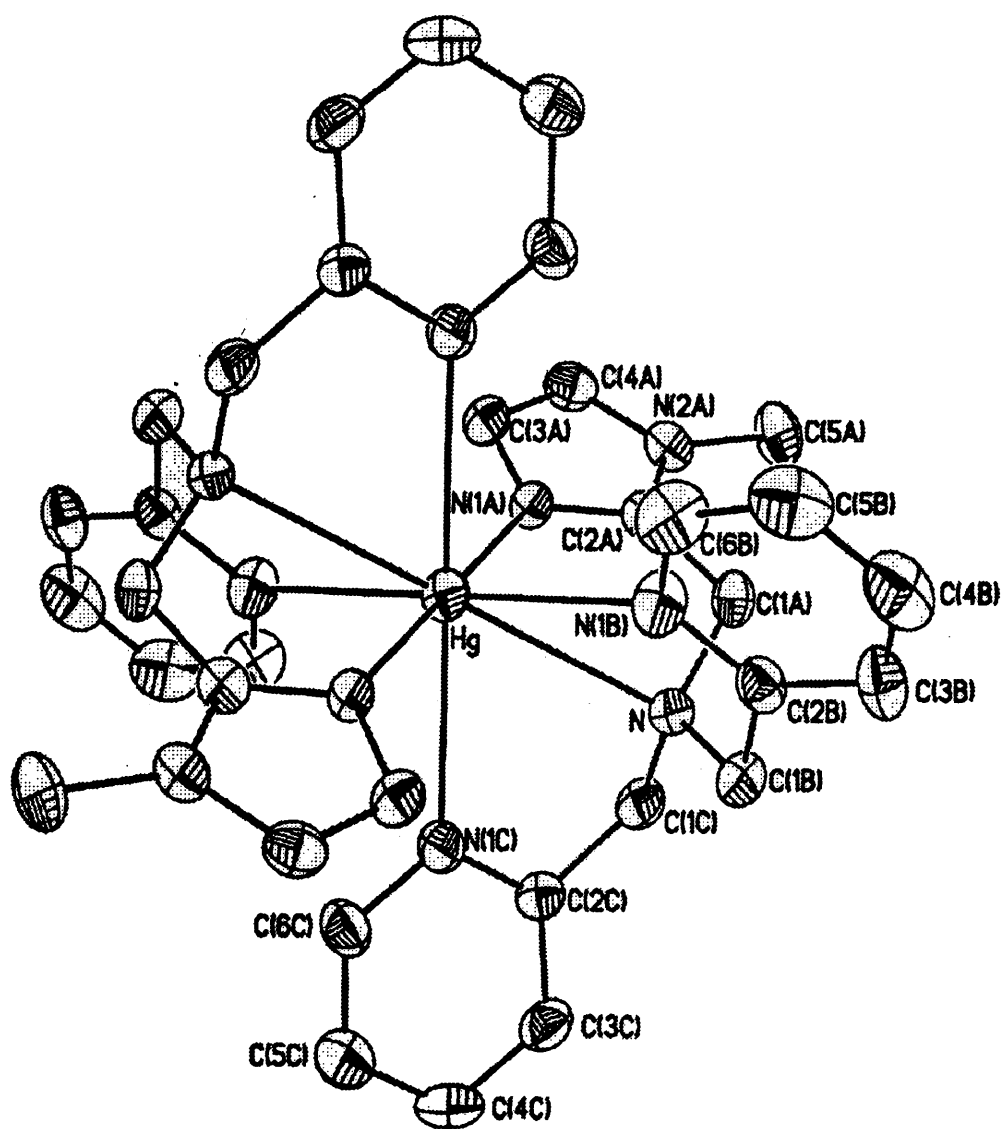
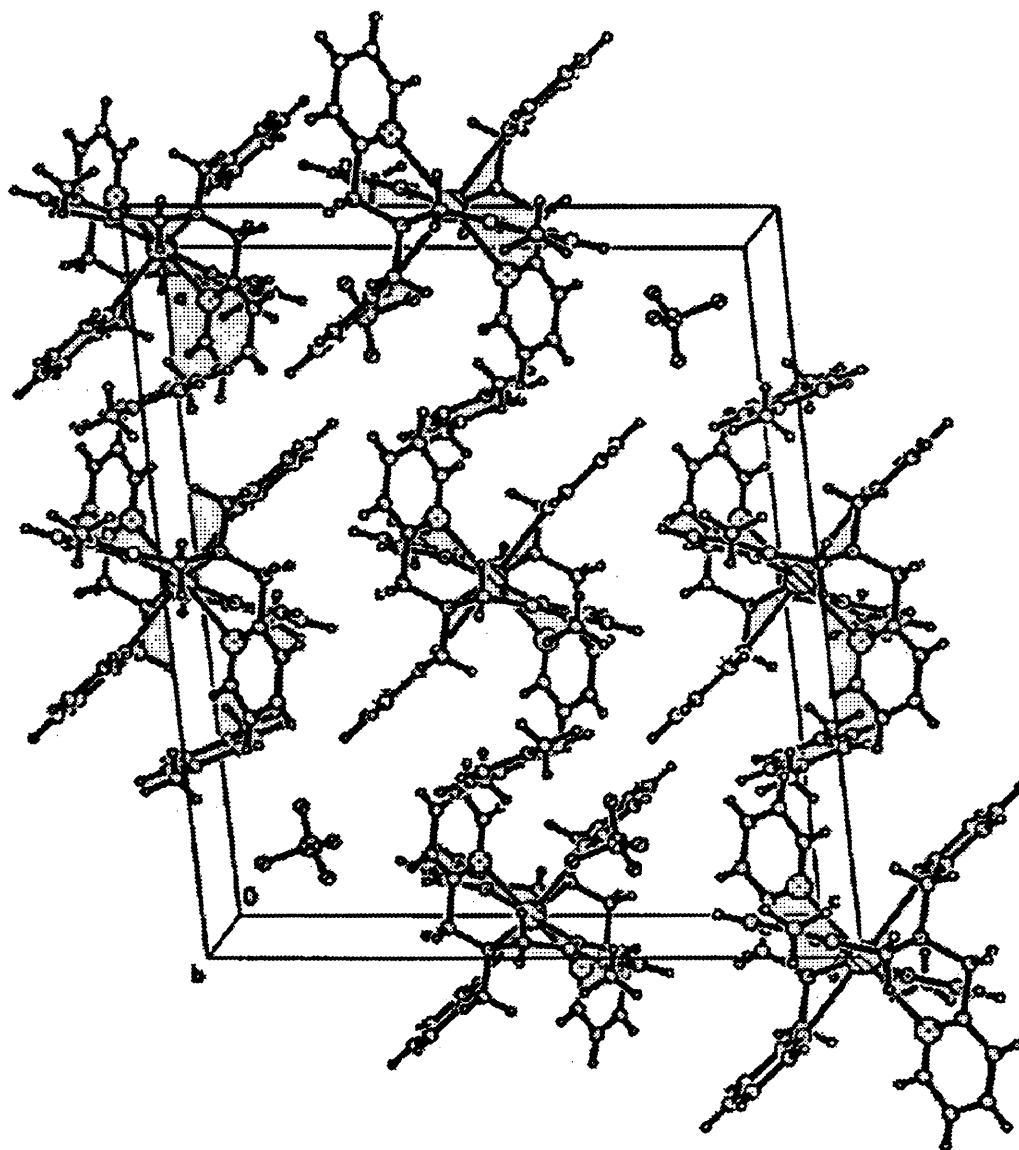**Figure 11.** Thermal Ellipsoid Representation of $[Hg(BPIA)_2]^{2+}$

Figure 12. Unit Cell Representation of [Hg(BPIA)₂](ClO₄)₂ • toluene

Table 1: Selected Crystallographic Data

	[Hg(BPIA)$_2$](ClO$_4$)$_2$ • toluene	[Hg(B-MIMA)Cl$_2$]
empirical formula	C$_{41}$H$_{46}$N$_{10}$Cl$_2$O$_8$Hg	C$_{10}$H$_{15}$N$_5$Cl$_2$Hg
fw	1077.36	476.76
space group	monoclinic, c2/c	monoclinic, P2$_1$/c
a, Å	21.4151(18)	12.055(3)
b, Å	11.8611(10)	8.9660(9)
c, Å	17.6893(15)	13.5517(14)
α, deg	90	90
β, deg	96.467(7)	98.827(18)
γ, deg	90	90
V, Å^3	4464.6(7)	1447.4(4)
Z	4	4
d$_{calc}$, Mg/m^{-3}	1.603	2.188
μ, mm^{-1}	3.630	10.933
radiation(monochromatic)	Mo Kα (l = 0.71073 Å)	Mo Kα (l = 0.71073 Å)
T, °C	20	20
R1[a]	0.0550	.0396
R2[b]	0.1341	.0653

[a] R1 = $\Sigma| |F_o| - |F_c| |/\Sigma|F_o|$. [b] R2 = $[\Sigma[w(F_o^2 - F_c^2)^2]/\Sigma[w(F_o^2)^2]]^{1/2}$.

Table 2: Selected Bond Distances (Å) in [Hg(BPIA)₂](ClO₄)₂ • toluene and [Hg(B-MIMA)Cl₂]

[Hg(BPIA)₂](ClO₄)₂ • toluene		[Hg(B-MIMA)Cl₂]	
Hg-N	2.829(5)	Hg-N	2.640(6)
Hg-N*	2.829(5)	Hg-N(1A)	2.250(6)
Hg-N(1A)	2.159(5)	Hg-N(1B)	2.293(6)
Hg-N(1A)*	2.159(5)	Hg-Cl(1)	2.524(2)
Hg-N(1B)	2.884(5)	Hg-Cl(2)	2.459(2)
Hg-N(1B)*	2.884(5)		
Hg-N(1C)	2.702(5)		
Hg-N(1C)*	2.702(5)		

Table 3: Selected Bond Angles (deg) in [Hg(BPIA)₂](ClO₄)₂ • toluene and [Hg(B-MIMA)Cl₂]

[Hg(BPIA)₂](ClO₄)₂ • toluene [a]		[Hg(B-MIMA)Cl₂]	
N-Hg-N*	180.0(2)	N-Hg-N(1A)	68.8(2)
N-Hg-N(1A)	66.4(2)	N-Hg-N(1B)	69.31(19)
N-Hg-N(1A)*	113.6(2)	N(1A)-Hg-N(1B)	131.8(2)
N-Hg-N(1B)	58.4(2)	N(1A)-Hg-Cl(1)	96.57(16)
N-Hg-N(1B)*	121.6(2)	N(1A)-Hg-Cl(2)	112.28(17)
N-Hg-N(1C)	62.8(2)	N(1B)-Hg-Cl(1)	100.76(16)
N-Hg-N(1C)*	117.2(2)	N(1B)-Hg-Cl(2)	103.26(17)
N(1A)-Hg-N(1A)*	180.0(2)	N-Hg-Cl(1)	140.47(15)
N(1A)-Hg-N(1B)	100.1(2)	N-Hg-Cl(2)	109.41(15)
N(1A)-Hg-N(1B)*	79.9(2)	Cl(1)-Hg-Cl(2)	110.12(8)
N(1A)-Hg-N(1C)	98.6(2)		
N(1A)-Hg-N(1C)*	81.4(2)		
N(1B)-Hg-N(1B)*	180.0(2)		
N(1B)-Hg-N(1C)	102.0(2)		
N(1B)-Hg-N(1C)*	78.0(2)		
N(1C)-Hg-N(1C)*	180.0(2)		

[a] Symmetry transformation used to generate equivalent atoms is #1) −x+1, -y+1, -z+1; #2) −x+1/2, -y+3/2, -z+1.

32

Crystal Structure of [Hg(B-MIMA)Cl$_2$]

This complex was made by evaporation of acetonitrile from a 1:1 ratio of mercury chloride and B-MIMA. A thermal ellipsoid diagram of the complex is given in Figure 13, a unit cell diagram in Figure 14, general crystallographic information is summarized in Table 1, selected bond lengths are given in Table 2, and selected bond angles are given in Table 3.

The complex is five-coordinate, and all donor nitrogens are part of a single chelating ligand. Two of the coordinating atoms are chlorine. The Hg-N$_{amine}$ bond distance is the longest bond measuring 2.640(6) Å. The 2.492(3) Å average Hg-Cl bond distance is longer than the Hg-N$_{imidazole}$ bond distance.

Other compounds have been studied with B-MIMA as part of the coordination environment. Oberhausen *et al.*, were able to obtain the five-coordinate complex [Cu(B-MIMA)(CH$_3$COO)](ClO$_4$).[15] In this species, the Cu-N$_{amine}$ bond distance was 2.047(2) Å and the average Cu-N$_{imidazole}$ bond distance was 1.971(4) Å. While these bonds are considerable shorter than those with mercury(II), the size of the metal ion is the most likely cause for the difference. Another six-coordinate B-MIMA complex reported in the literature is [Fe(B-MIMA)(acetic acid)Cl$_2$].[21] In this complex, the Fe-N$_{amine}$ bond distance is 2.32(2) Å and the average Fe-N$_{imidazole}$ bond distance is 2.10(2) Å. These numbers are similar to the complex reported here and again the metal ion may be the determining factor in coordination strength.

The mercury(II) complex of B-MIMA can be more directly compared to the five-coordinate complex [Hg(TLA)Cl$_2$] (TLA=tris[(6-methyl-2-pyridyl)methyl]amine) in which one of the pyridyl rings of TLA is pendant.[24] Both complexes exhibit a metal

coordination sphere of a distorted trigonal bipyramid. All of the Hg-N bond lengths are similar in the TLA complex (as well as other synthesized pyridyl complexes) but large differences are present in the B-MIMA complex. The Hg-N$_{amine}$ bond distance for the TLA complex is 2.505(7) Å which is shorter than the Hg-N$_{amine}$ distance of 2.640(6) Å in the B-MIMA complex. The average TLA Hg-N$_{pyridyl}$ bond distance is 2.496(9) Å which is longer than the average Hg-N$_{imidazole}$ bond distance of 2.292(8) Å in B-MIMA. The comparison of these two complexes shows that the imidazoyl rings adopt a similar conformation to the more commonly used pyridyl rings.
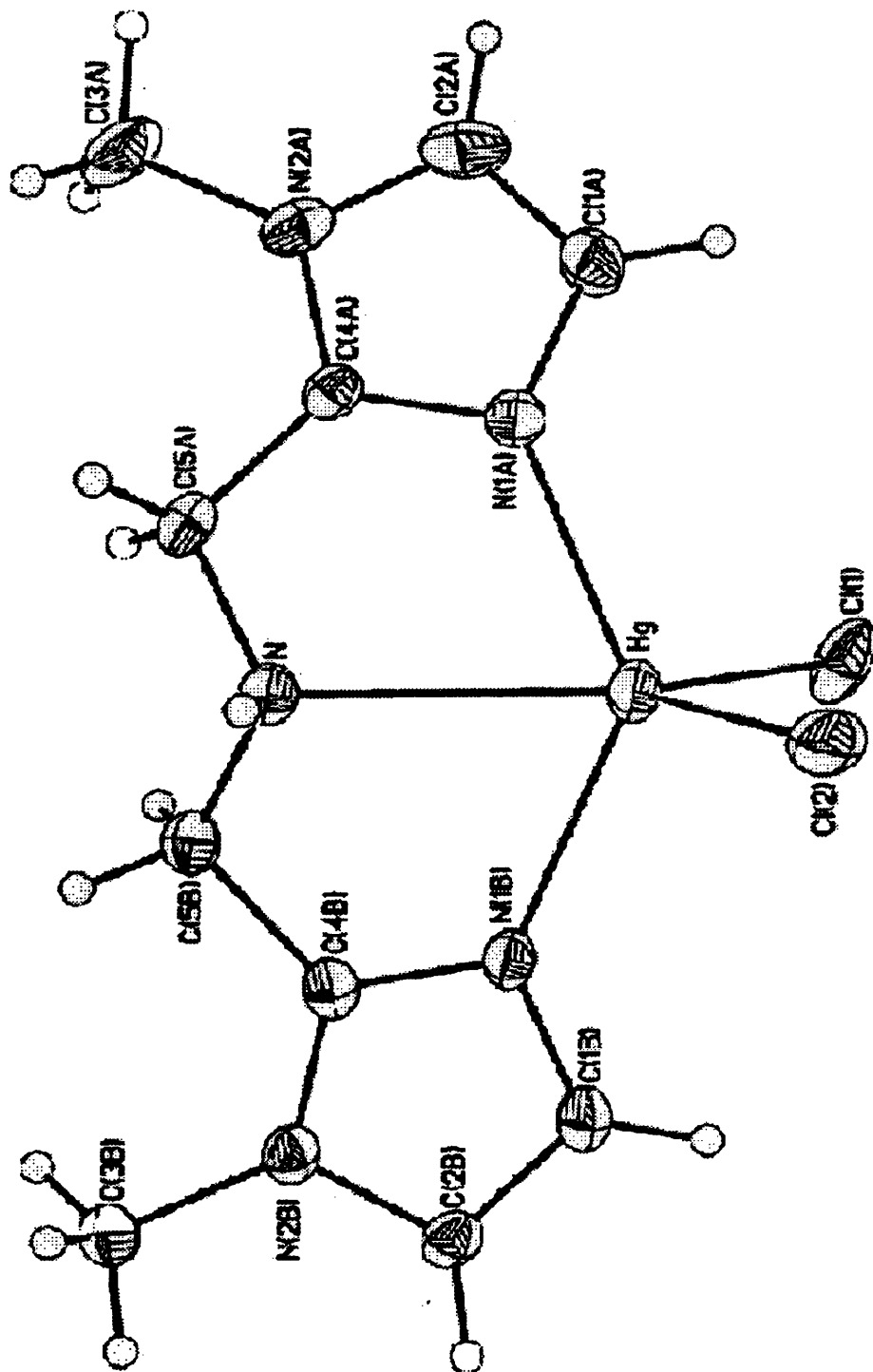
Figure 13. Thermal Ellipsoid Representation of [Hg(B-MIMA)Cl₂]
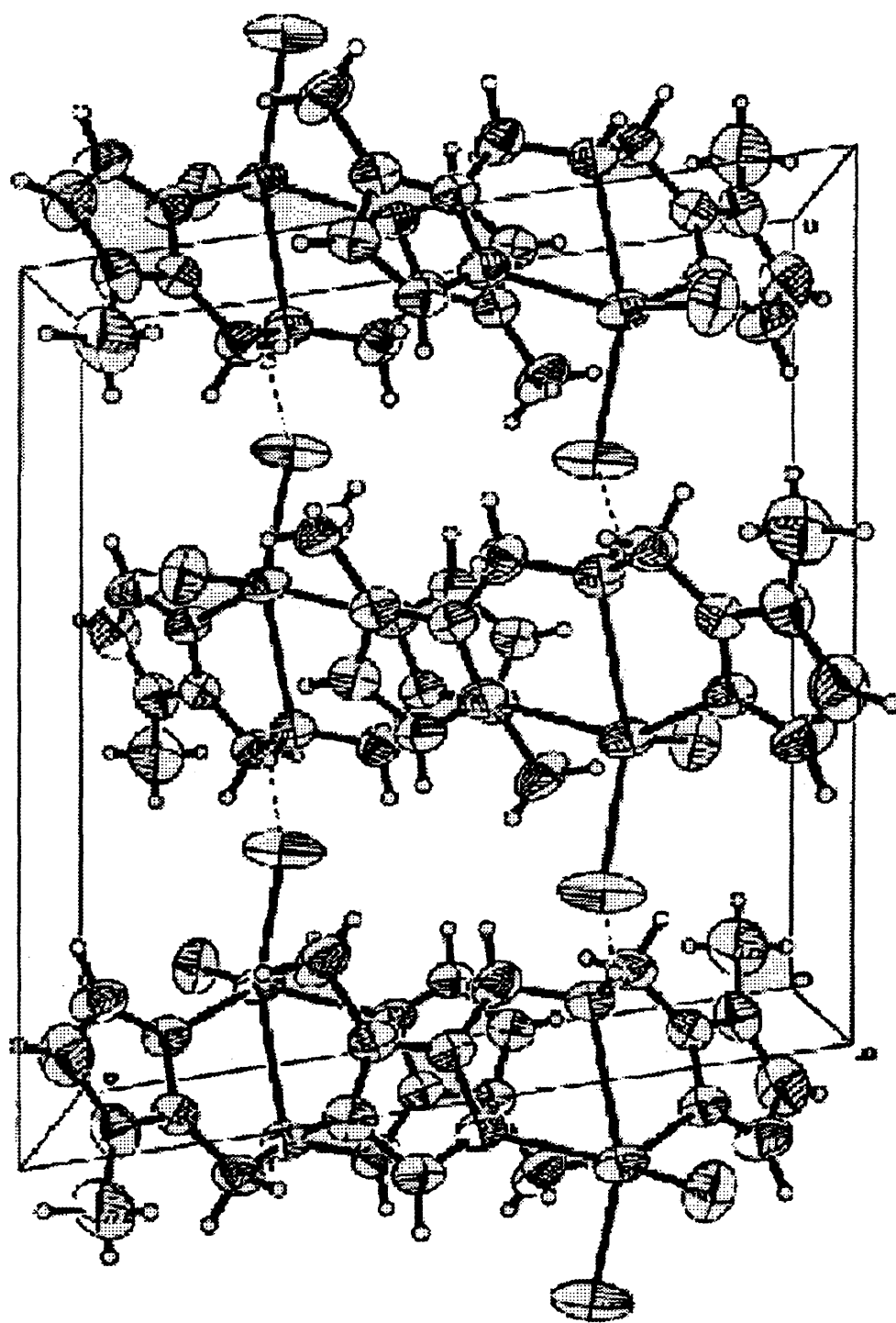
Figure 14. Unit Cell Representation of [Hg(B-MIMA)Cl₂]

III. NMR SOLUTION-STATE STUDIES OF HG(II) COORDINATION

Solution-State Investigations of BPIA

A series of solutions in which the Hg:BPIA ratio was increased from 0 (free ligand) to 2:1 with 2 mM mercury perchlorate were prepared in acetonitrile-d_3. Proton NMR was performed on these solutions at -40 °C. Figure 15 shows a plot of chemical shift vs. metal-to-ligand ratio of selected hydrogen atoms in the aromatic region, while Figure 16 plots the same NMR runs in the methyl/methylene region. Figure 17 shows a stacked plot of proton NMR spectra at selected metal-to-ligand ratios.

At metal-to-ligand ratios below 0.625, resonances for free ligand and one additional species assigned to the 1:2 metal-to-ligand complex were observed. The relative intensity of the resonances associated with this complex are greatest near [Hg]/[BPIA] = 0.5. At higher metal-to-ligand ratios, a new complex believed to be the 1:1 metal-to-ligand complex begins to appear. At metal-to-ligand ratios greater than 1.0, only resonances for the later complex are observed. Figures 15 and 16 show the significant difference in chemical shifts of the two proposed species. It should be noted that the two hydrogens which experience the greatest difference in chemical shift are the hydrogens closest to the coordinating nitrogen groups of both the pyridyl (H_A) and imidazole rings (H_K). The near consistency of the chemical shift values for the two metal complexes indicates they are in slow exchange with free ligand and each other in the chemical shift time scale and that no other species contribute significantly to solution equilibrium.

Coupling to the two imidazoyl nitrogens was also observed within this NMR series. Figure 18 shows a plot of the observed coupling constants versus metal-to-ligand ratio. As shown in the plot, the imidazoyl protons (H_K and H_L) have $^3J(^1H^{199}Hg)$ of 34 and 36 Hz in the 1:2 [Hg]/[BPIA] complex and 19 and 27 Hz in the 1:1 [Hg]/[BPIA] complex. Although some scatter is observed in the recorded coupling constants, they appear to be independent of [Hg]/[BPIA] which is consistent with slow exchange on the coupling constant time scale. It should also be pointed out that one of the coupling satellites for each imidazoyl peak coincided in-between the two imidazoyl signals at metal-to-ligand ratios above 1.0 (Figure 17, inset d). As a result these coupling constants may not be as precise.

It is interesting to note the difference in coupling patterns between BPIA and TMPA. In the 1:2 complex, [Hg(TMPA)$_2$](ClO$_4$)$_2$, coupling is present for only the methylene protons, and has a magnitude of 46 Hz.[23] For the 1:1 complex, [Hg(TMPA)](ClO$_4$)$_2$, both the hydrogen adjacent to the coordinating pyridyl nitrogen and the methylene hydrogens show coupling, with magnitudes of 40 and 36 Hz, respectively. While the imidazoyl hydrogens, H_K and H_L, in BPIA show coupling for both the 1:1 and 1:2 complexes, coupling of pyridyl protons only appears in the 1:1 TMPA and 1:1 BPIA complexes. The magnitude of coupling for the methylene protons in TMPA decreases for the lower coordination number complex in a similar fashion to the imidazole proton H_K and H_L in the BPIA complexes. The longer bond distance for the pyridyl rings of BPIA compared to TMPA in the 1:2 complexes may account for the lack of coupling present for the pyridyl rings of BPIA. At metal-to-ligand ratios greater than 1.0, proton H_A shows a coupling constant of 35 Hz which is also split into a doublet. This coupling may

be obscured in higher metal-to-ligand ratios due to a new species appearing in the spectra. No coupling to the methylene protons of BPIA was noted possibly due to the long Hg-N$_{amine}$ bond length.
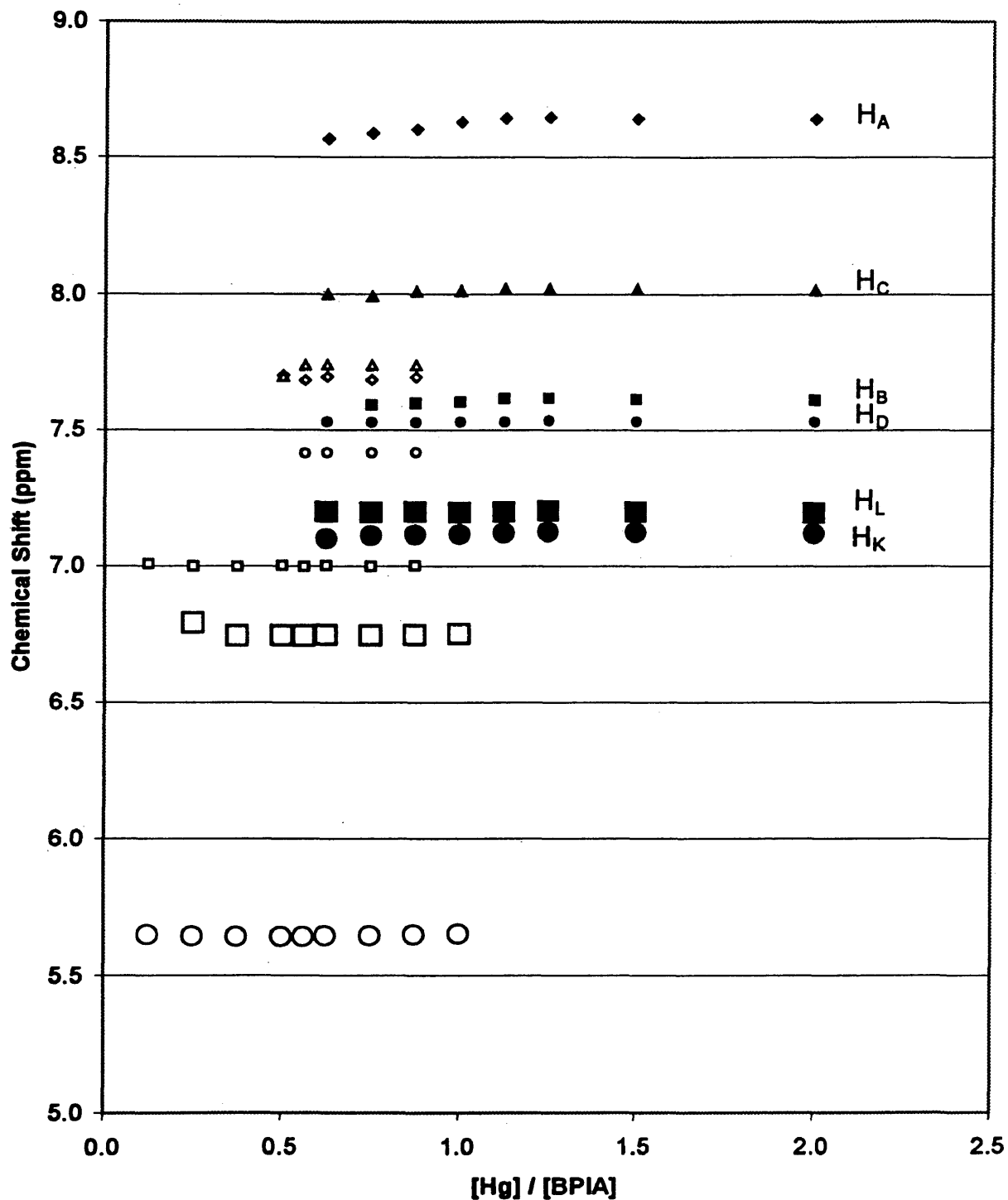
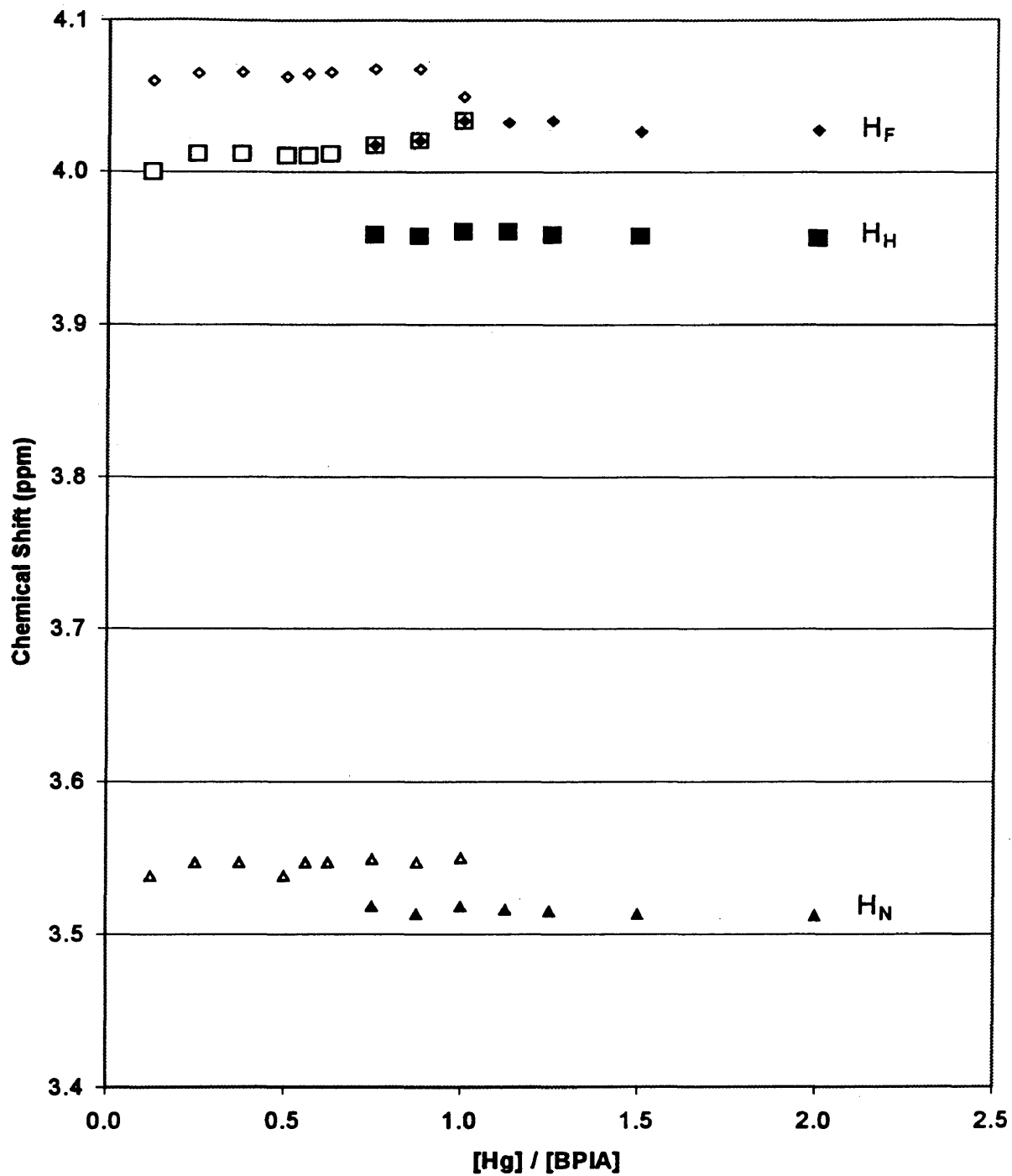**Figure 15.** Chemical shifts of aromatic protons in BPIA in the presence of $Hg(ClO_4)_2$ as a function of metal-to-ligand ratio in CD_3CN at −40 °C. Open symbols represent the proposed 1:2 complex and closed symbols represent the proposed 1:1 complex. Total metal concentration was 2 mM. Resonances associated with free ligand omitted for clarity.

Figure 16. Chemical shifts of methyl/methylene protons in BPIA in the presence of $Hg(ClO_4)_2$ as a function of metal-to-ligand ratio in CD_3CN at -40 °C. Open symbols represent the proposed 1:2 complex and closed symbols represent the proposed 1:1 complex. Total metal concentration was 2 mM. Resonances associated with free ligand omitted for clarity.
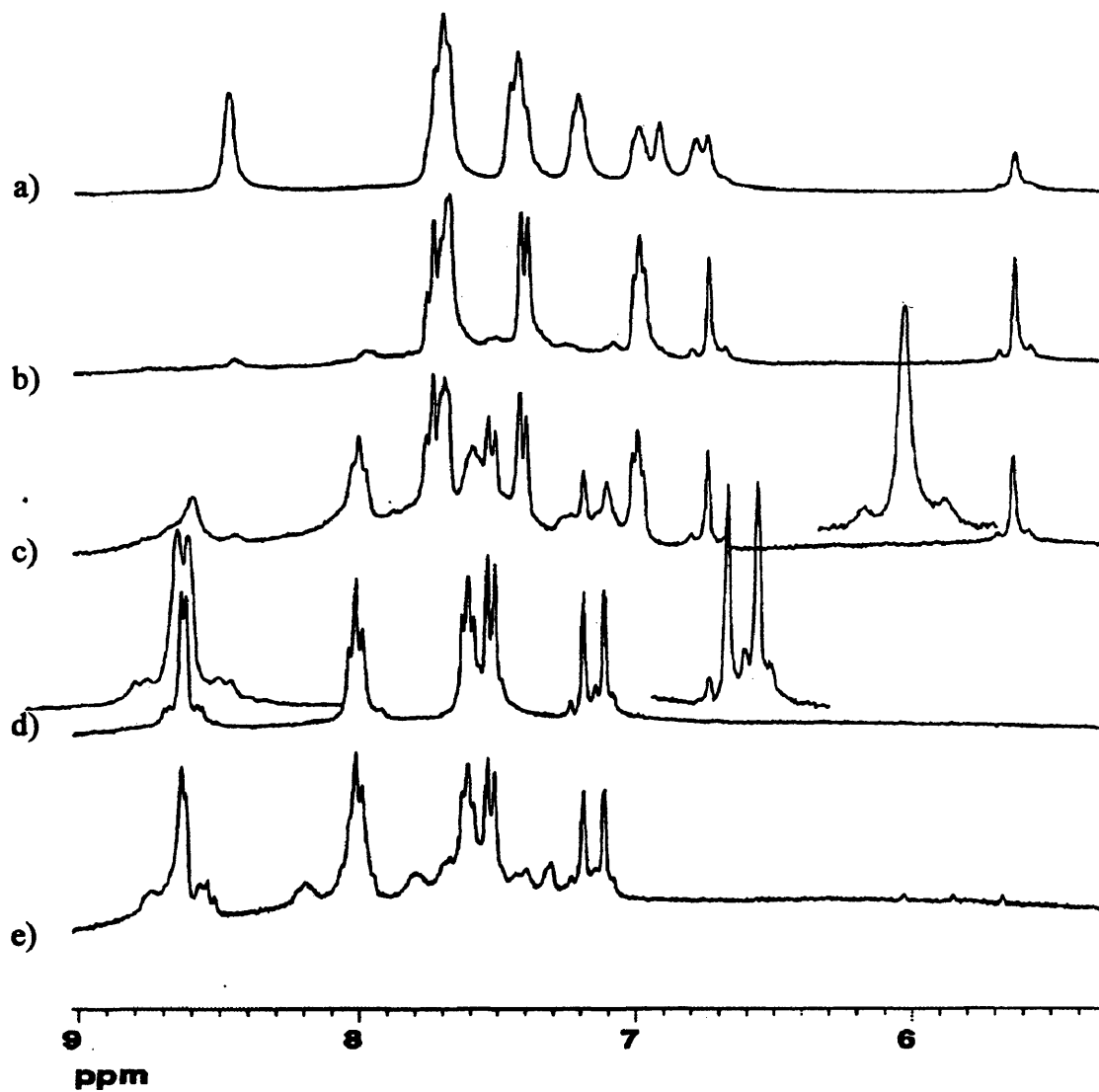
Figure 17. Stack plot of several NMR spectra of BPIA in the presence of $Hg(ClO_4)_2$ at –40 °C in CD_3CN. Total metal concentration was 2 mM. Metal-to-ligand ratios = a) 0.250, b) 0.5625, c) 0.750, d) 1.125, e) 2.00
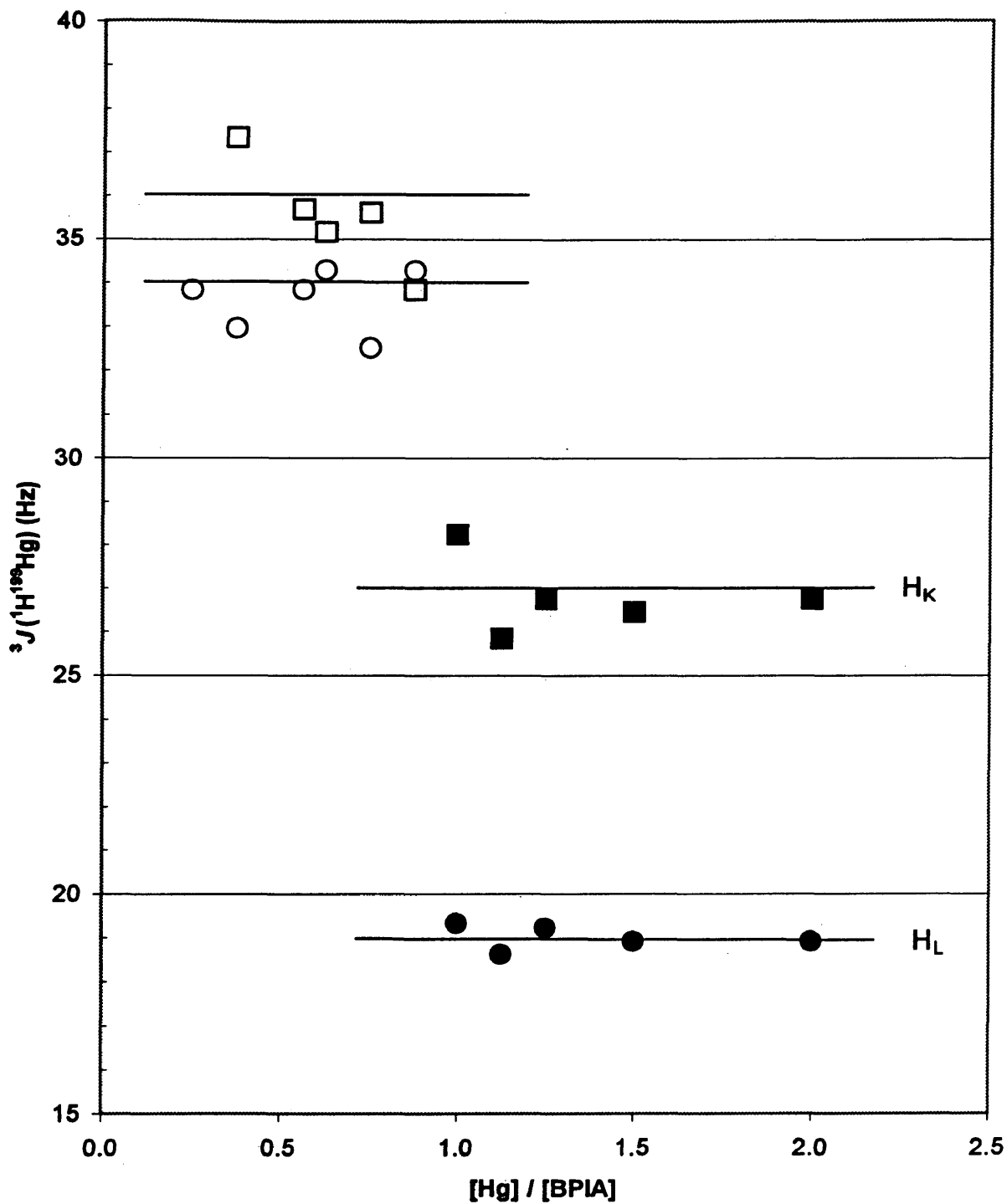
Figure 18. Magnitude of coupling constants of the imidazole protons of BPIA in the presence of $Hg(ClO_4)_2$ as a function of metal to ligand ratio at $-40°$ C. The total metal concentration was 2 mM. Open symbols represent proposed 1:2 complex and closed symbols represent proposed 1:1 complex. Lines represent average coupling constant value.

Solution-State Investigations of B-MIMA

Two separate series in which the Hg:B-MIMA ratio was increased from 0 (free ligand) to 2:1 in acetonitrile-d_3 were recorded. The first series used mercury chloride and the second mercury perchlorate. Proton NMR was performed on these solutions at -40 °C. For the mercury chloride series, Figure 19 shows a plot of chemical shift vs. metal-to-ligand ratio of selected hydrogen atoms in the aromatic region, while Figure 20 plots the same NMR runs in the methyl/methylene region. Figure 21 shows a stacked plot of proton NMR spectra at selected metal to ligand ratios. For the mercury perchlorate series, Figure 22 shows a stacked plot of proton NMR spectra at selected metal-to-ligand ratios.

The resonances for the methyl protons (H_D) were nearly unchanged throughout the $HgCl_2$ series but the other protons experience shifts between 0.201 and 0.322 ppm. The later chemical shifts increase steeply and approximately linearly up to a metal-to-ligand ratio of 1.0. This suggests formation of [Hg(B-MIMA)Cl$_2$] in solution. In this region of the titration, the weighted average of the chemical shifts is expected to be described by eq 1

$$\delta_{obs} = P_{free}\delta_{free} + (1 - P_{free})\delta_{1:1} \qquad (1)$$

where δ_{free} and $\delta_{1:1}$ are the chemical shifts and P_{free} and $P_{1:1}$ [$(1 - P_{free})$] are the mole fractions of free ligand and the 1:1 metal-to-ligand complex.[24] At ratios greater than one a different slope exists, possibly representing multinuclear complexes. Since multinuclear complexes are of limited biological relevance no attempts to further characterize complexes after metal-to-ligand ratio of 1.0 was made. Coupling was not observed in this series. Future studies, i.e. [Hg(B-MIMA)Cl$_2$] plus small amounts of

metal and/or ligand, will attempt to determine whether rapid exchange rates or resolution limits obscure coupling.

The $Hg(ClO_4)_2$ series had a single set of exchange averaged chemical shifts at metal-to-ligand ratios less than 0.5625, consistent with formation of a 1:2 metal-to-ligand complex in equilibrium with free ligand. At higher metal-to-ligand ratios, the spectra were very complex, although a single major species could be discerned at metal-to-ligand ratios greater than 1.125. Resonances for six minor components were observed. Coupling was not observed in this series. Interestingly, the related tridentate ligand BMPA (bis[(2-pyridyl)methyl]amine) exhibited very different behavior under similar conditions with $Hg(ClO_4)$.[25] In this study the complexes $[Hg(BMPA)_2](ClO_4)_2$ •0.5toluene and $[Hg(BMPA)NCCH_3](ClO_4)_2$ were correlated with solution state NMR spectra. BMPA exhibits well-resolved $^3J(^1H^{199}Hg)$ for the pyridyl proton next to the coordinating nitrogen and the methylene protons next to the coordinating amine. This coupling was observed both at room temperature for the 1:1 complex and at −40 °C for the 1:2 complex. The low temperature conditions allowed for identification of mercury-proton coupling below metal-to-ligand ratios of 0.5 and the large magnitudes of these coupling constants suggest they arise through three-bond coupling rather than longer range interactions. Preliminary data on the structure of $[Hg(B-MIMA)_2](ClO_4)_2$ appears to show that one of the imidazoyl rings on one B-MIMA molecule is pendant. This could be a reason that coupling is not observed for the imidazoyl hydrogens if there is rapid exchange of bound imidazoyl rings to the mercury(II) ion. However, coupling should still be detectable for the methylene hydrogens if the $Hg-N_{amine}$ bond is stable on the NMR time scale.
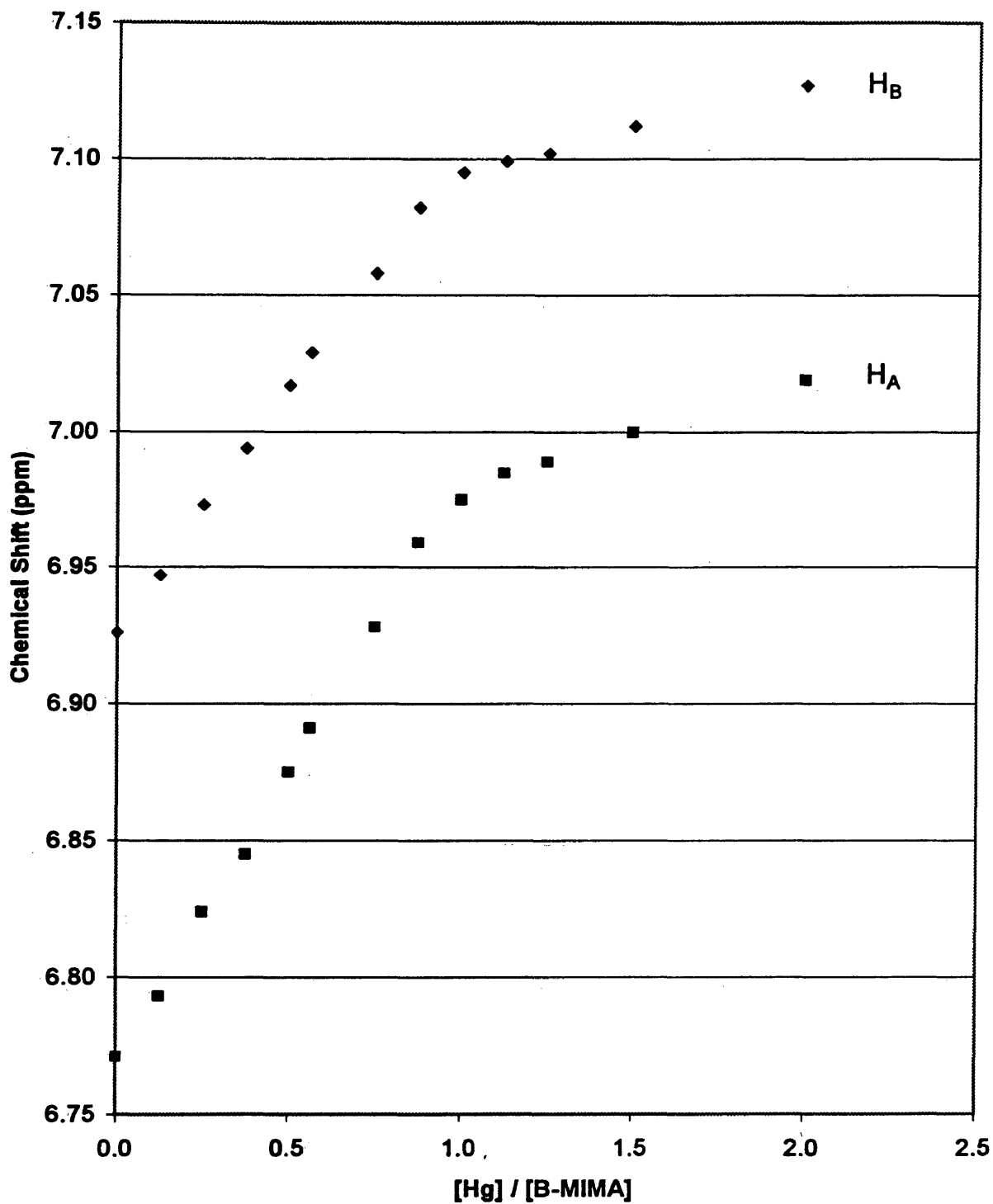
45

Figure 19. Chemical shifts of aromatic protons in B-MIMA in the presence of HgCl₂ as a function of metal to ligand ratio in CD₃CN at −40 °C. Total metal concentration was 2 mM.
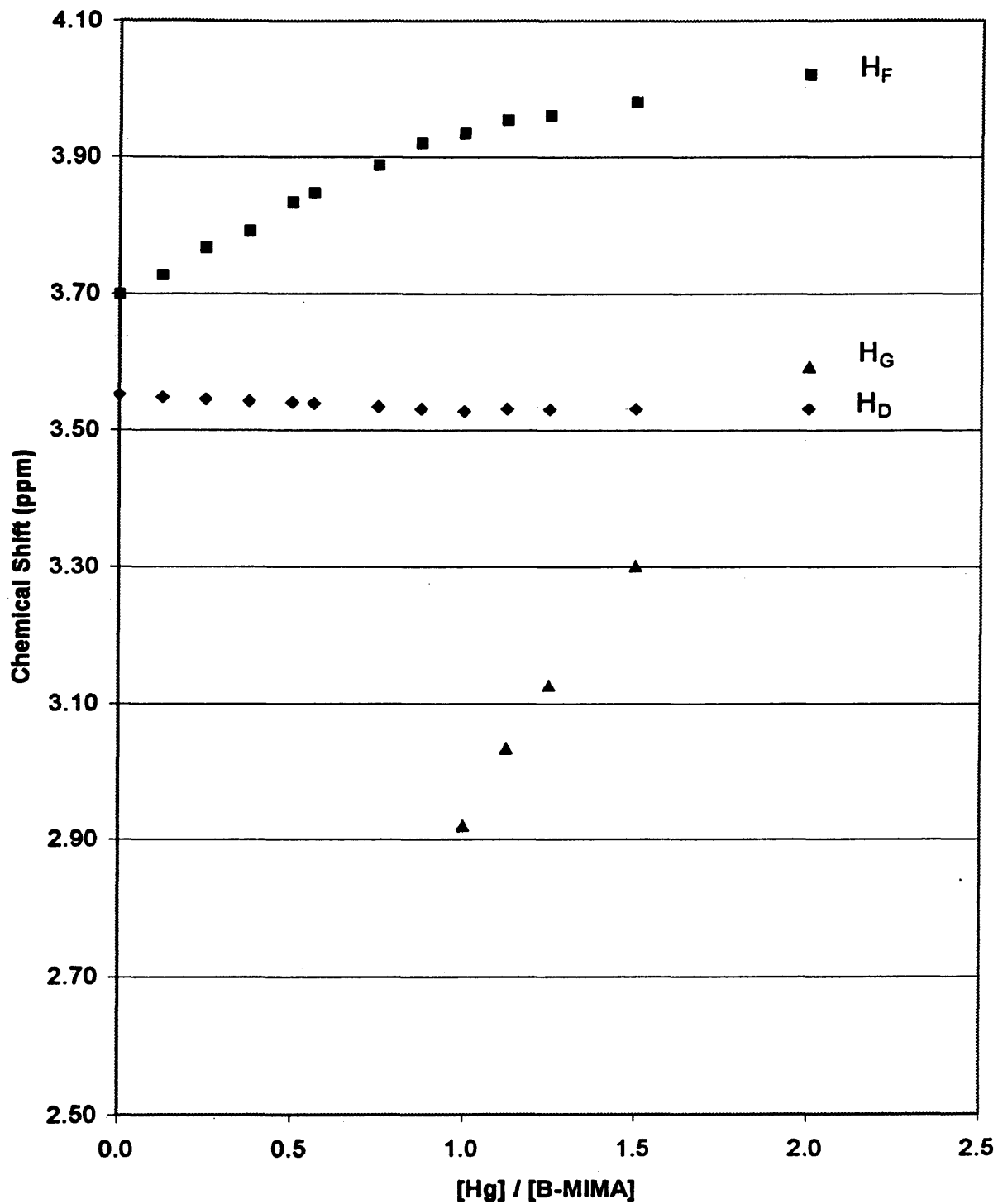
Figure 20. Chemical shifts of methyl/methylene protons in B-MIMA in the presence of $HgCl_2$ as a function of metal to ligand ratio in CD_3CN at -40 °C. Total metal concentration was 2 mM.
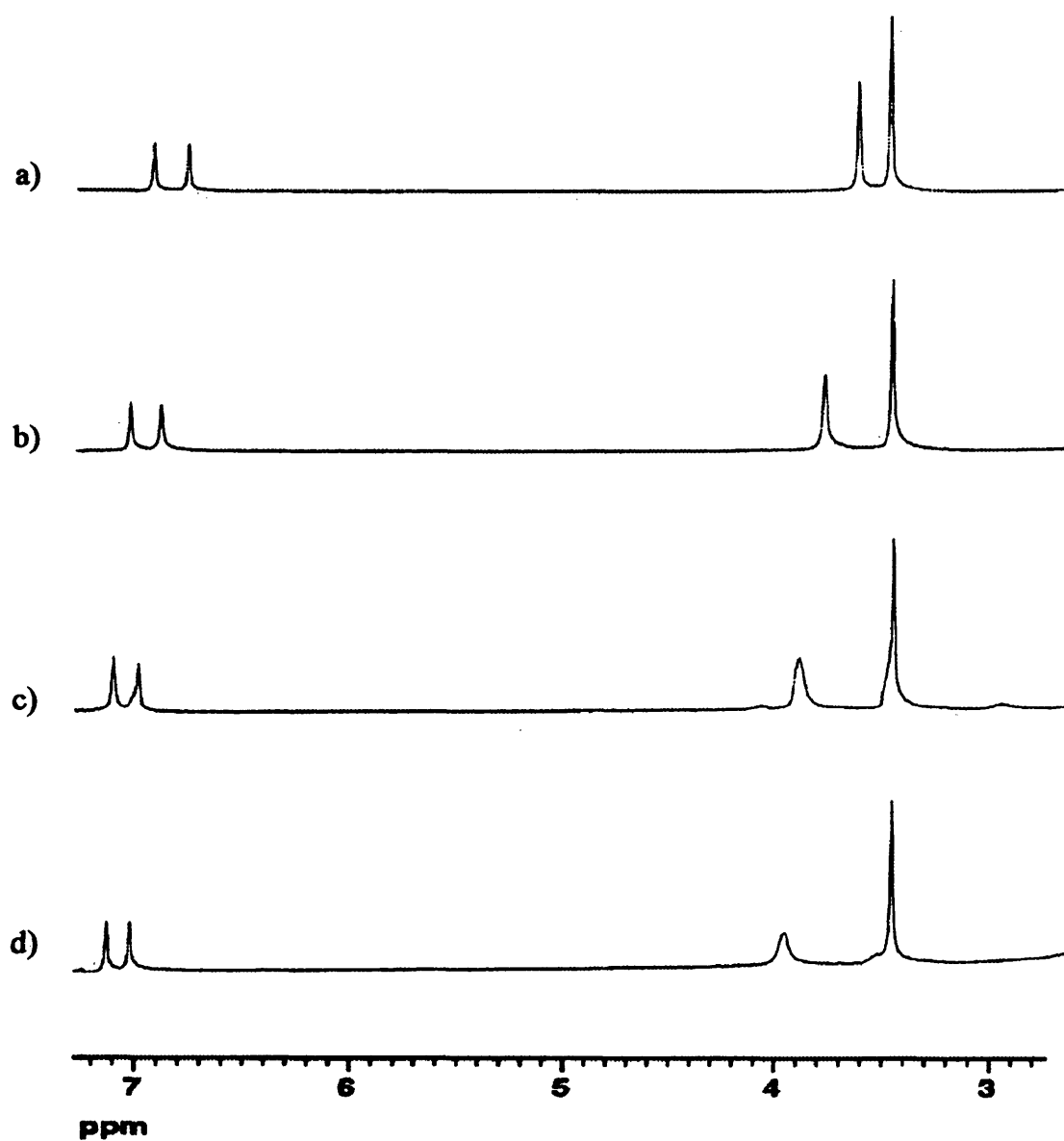
Figure 21. Stack plot of several NMR spectra of B-MIMA in the presence of HgCl₂ at –40 °C in CD₃CN. Total metal concentration was 2 mM. Metal-to-ligand ratios = a) free ligand, b) 0.5625, c) 1.125, d) 2.0
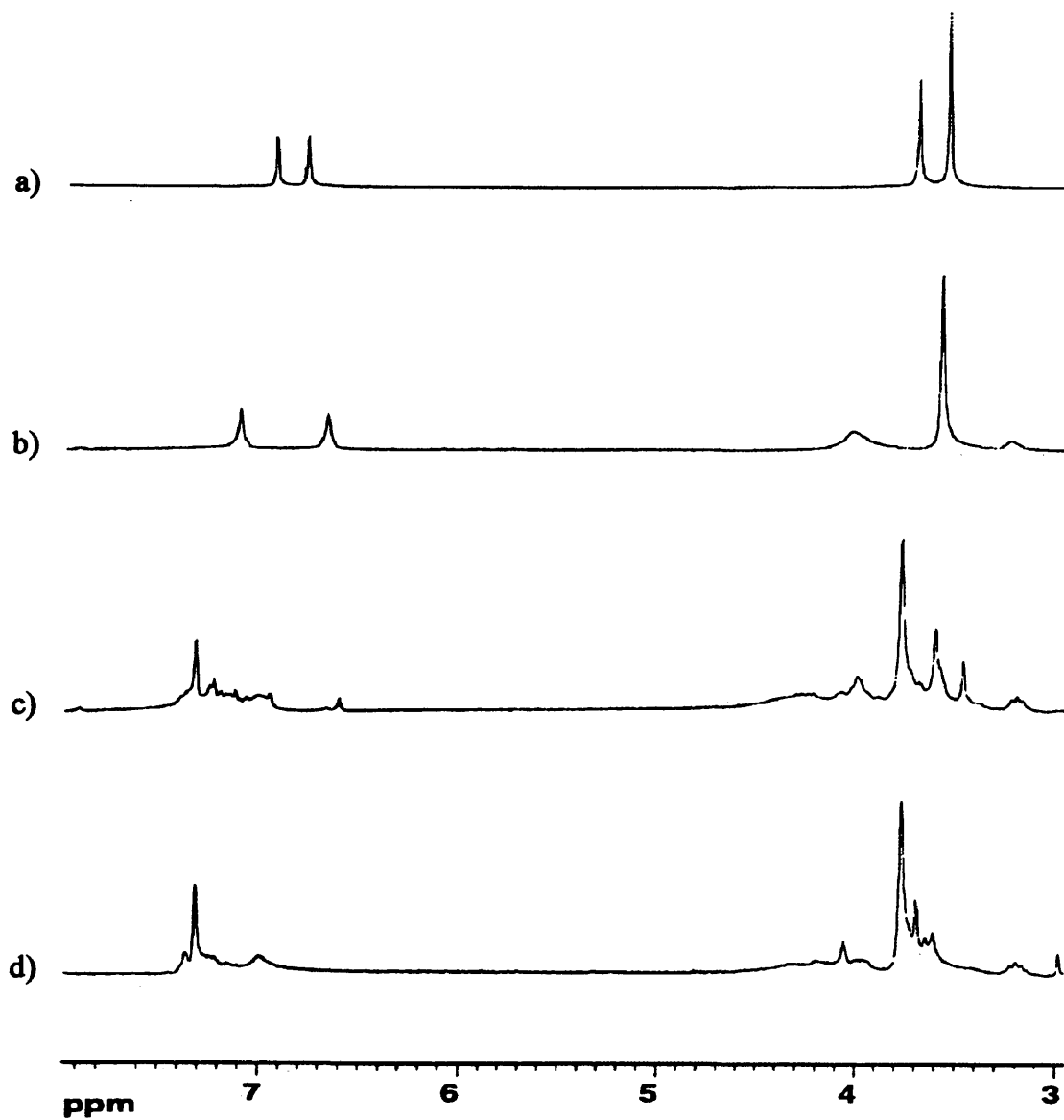
Figure 22. Stack plot of several NMR spectra of B-MIMA in the presence of Hg(ClO₄)₂ at -40° C in CD₃CN. Total metal concentration was 2 mM. Metal-to-ligand ratios = a) free ligand, b) 0.5625, c) 1.0, d) 1.5

CONCLUSION

Using small, organic ligands to model amino acids, recent studies have suggested that [199]Hg NMR may be a useful probe of protein metal binding sites. This study has expanded upon past research with pyridyl ligands and started introducing imidazoyl ligands into these mercury studies. The comparison of mercury complexes with the organic ligands BPIA and B-MIMA allows for investigation of heteronuclear coupling between the metal and proton. In the case of BPIA, solution state coupling was observed between the imidazoyl hydrogens and mercury. In addition, the crystallographic data presents an opportunity to explore correlation between solid-state characteristics and the solution-state properties. Combining these two analytical techniques, information about the metal ion and protons within the surrounding ligands can be used to characterize the metal ion environment.

In the case of the $[Hg(BPIA)_2](ClO_4)_2$ complex, the crystallographic information shows that the imidazoyl ring is more tightly bound than the pyridyl rings. This could explain why only the imidazole hydrogens showed any coupling in the solution-state NMR studies. The magnitudes of the spin-spin coupling constants are influenced by various factors. Three-bond coupling constants are commonly related to molecular structure through a Karplus-type relationship:

$$^3J_{XY} = A\cos 2\phi + B\cos\phi + C \qquad (2)$$

where A, B and C are empirical constants and ϕ is the dihedral angle. Previous studies have suggested that $^3J(^1H^{199}Hg)$ has a Karplus-type relationship. However, other factors will contribute to observed coupling, such as, electronegativity and variation in bond lengths and angles. Previous studies in which $^3J(^1H^{199}Hg)$ were observed for Hg-N$_{pyridyl}$, had significantly shorter bond lengths than those observed with BPIA. Since similar geometries are present, this could be a strong contributing factor to the lack of coupling present with the pyridyl rings. In the case of [Hg(B-MIMA)Cl$_2$], no coupling was observed. This is surprising since the solid-state data suggests that this complex is very similar to the comparable Hg-TLA complex which did exhibit coupling. The lack of observed coupling may be caused by rapid exchange of B-MIMA compared to the NMR time scale.

Future efforts to continue the development of ^{199}Hg as a NMR metalloprobe will include investigation of new ligand systems and performing ^{199}Hg NMR on known complexes. Another series of ligands that are being examined are cyclic dipeptides. Cyclic dipeptides provide a model which uses the actual peptide bonds found in proteins. The chemical shift data library constructed by ^{199}Hg NMR of known complexes will be instrumental in characterization of new protein metal binding sites.

REFERENCES

1. Creighton, T.E. Proteins, 2nd Ed., Freeman, New York, 1993.

2. Anfinsen, C.B.; Haber, E.; Sela, M.; White, F.H. *Proc. Natl. Acad. Sci. USA* 1961, *47*, 1309-1314.

3. Thomas, P.J.; Qu, B.-H.; Pedersen, P.L. *TIBS* 1995, *20*, 456.

4. Voet, D.; Voet J.G. Biochemistry, 2nd Ed., John Wiley & Sons, Inc.: New York, 1995, p.376.

5. Balbach, J.; Forge, V., van Nuland, N.A.J.; Winder, S.L.; Hore, P.J.; Dobson, C.M. *Nature, Struct. Biol.* 1995, *2*, 865-870.

6. Vollhardt, K.P.C.; Schore, N.E. Organic Chemistry, W.H. Freeman and Company, New York, 1994, pp. 328-331.

7. Silverstein, R.M.; Webster, F.X. Spectrometric Identification of Organic Compounds, 6th Ed., John Wiley & Sons, Inc.: New York, 1998.

8. Church, B.W.; Guss, M.; Potter, M.J.; Freeman, H.C. *J. Biol. Chem*, 1986, *261*, 234-237.

9. Summers, M.F. *Coord. Chem. Rev.* 1988, *86*, 43-134.

10. Armitage, T.M.; Pajer, R.T.; Schoot Uiterkamp, A.J.M.; Chlebowski, J.F.; Coleman, J.G.; *J. Am. Chem. Soc.* 1976, *98*, 5710.

11. Cheesman, B.V.; Arnold, A.P.; Rabenstein, D.L.J. *Am. Chem. Soc.* 1988, *110*, 6359 and references sited therein.

12. Blake, P.R.; Lee, B.; Summers, M.F. *New J. Chem.* 1994, *18*, 387-395.

13. Utschig, L.M.; Wright, J.G.; Dieckmann, G.; Pecoraro, v.; O'Halloran, T.V. *Inorg. Chem.* 1995, *34*, 2497-2498.

14. Natan, M.J.; Millikan, C.F.; Wright, J.G.; O'Halloran, T.V. *J. Am. Chem.Soc.* 1990, *112*, 3255-3257.

15. Oberhausen, K.J.; Richardson, J.F.; Buchanan, R.M. *Polyhedron* **1989**, *8*, 659-668.

16. Wei, N.; Murthy, N.N.; Tyeklar, Z.; Karlin, K.D. *Inorg. Chem.* **1994**, *33*, 1177-1183.

17. Oberhausen, K.J.; Easley, W.D.; Richardson, J.F.; Buchanan, R.M. *Acta Cryst.* 1991, *C47*, 2037-2040.

18. *SHELXTL-Plus*, Version 4.21/V; Siemens Analytical X-ray Instruments, Inc.: Madison, WI, 1990.

19. *Sheldrick*, G.M. *Crystallographic Computing 6*; Flack, H.D., Parkanyi, L., Simon, K., Eds.; Oxford University Press: Oxford, 1993; p.111.

20. (a) Wosley, W.C. *J. Chem. Educ.*, **1973**, 50, A335. (b) Raymond, K.N. *Chem. Eng. News* **1983**, *61* (49), 4.

21. Rodriguez, M.C.; Morgenstren-Badarau, I.; Cesario, M.; Guilhem, J.; Keita, B.; Nadjo, L. *Inorg. Chem.* **1996**, *35*, 7804-7810.

22. Akesson, R.; Sandstrom, M.; Stalhandske, C.; Persson, I. *Acta Chem. Scand.* **1991**, *45*, 165.

23. Bebout, D.C.; Ehmann, D.E.; Trinidad, J.C.; Crahan, K.K. *Inorg. Chem.* **1997**, *36*, 4257-4264.

24. Bebout, D.C.; Bush, J.F.; Crahan, K.K. *Inorg. Chem.* **1998**, *37*, 4641-4646.

25. Bebout, D.C.; DeLanoy, A.E.; Ehmann, D.E. *Inorg. Chem.* **1998**, *37*, 2952-2959.
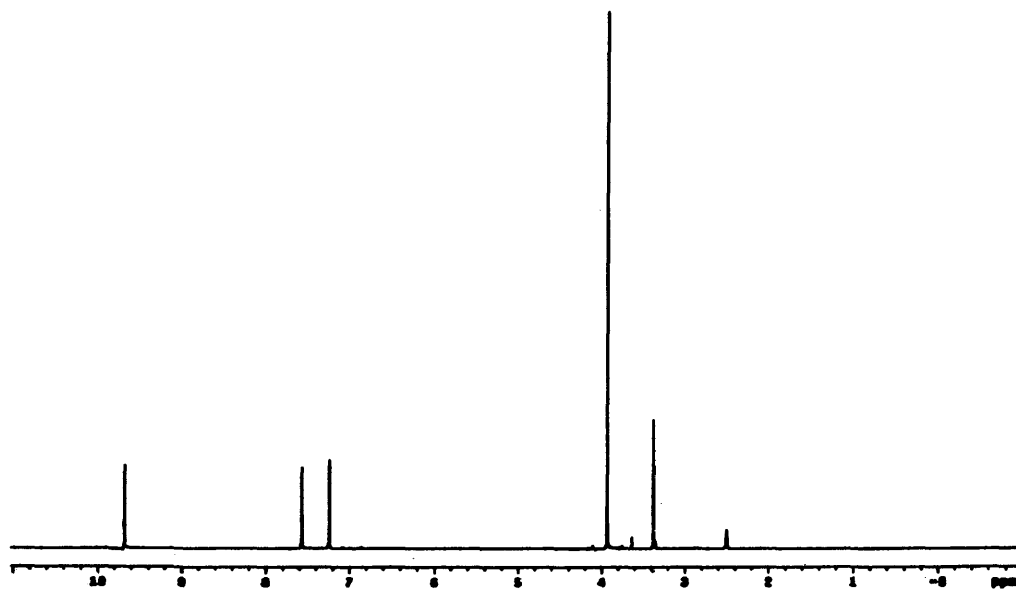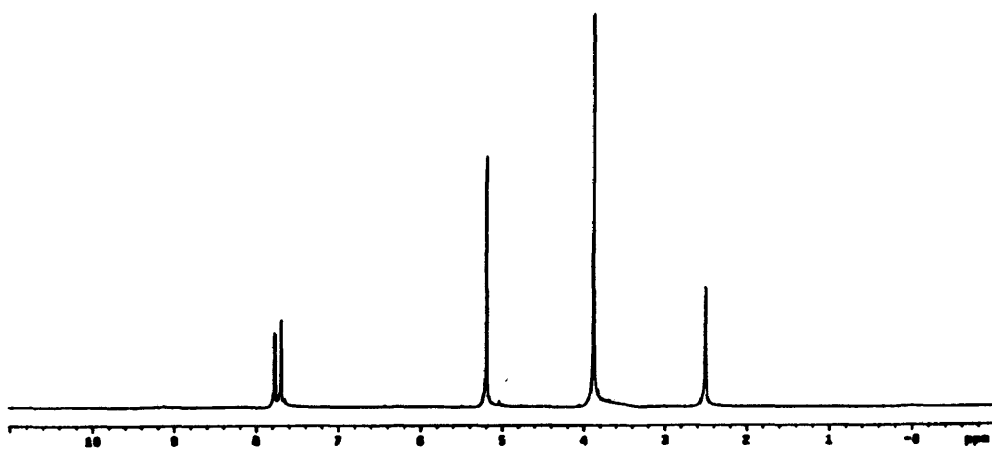
Appendix 1. ^{1}H NMR of MICA
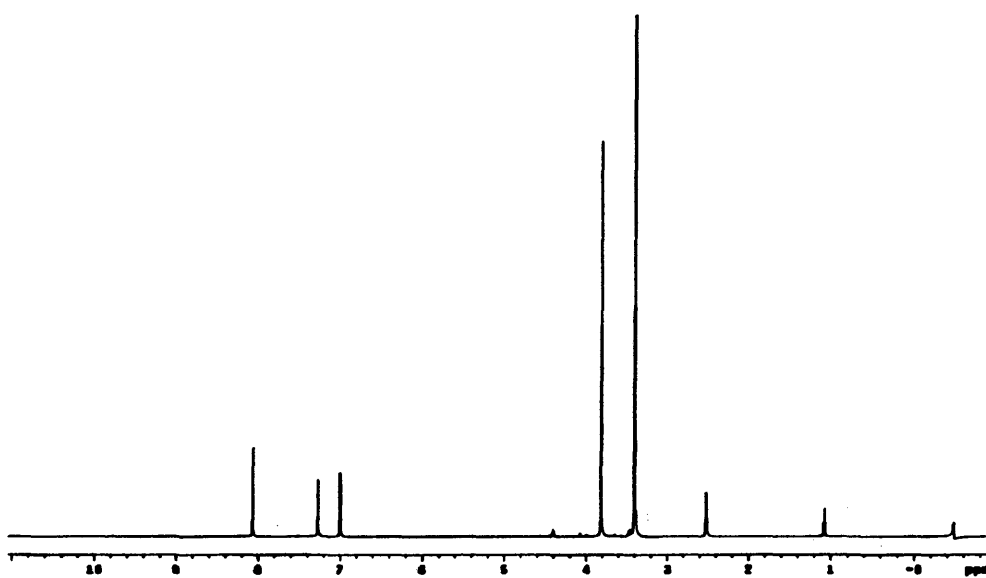
Appendix 2. ^{1}H NMR of MICAO
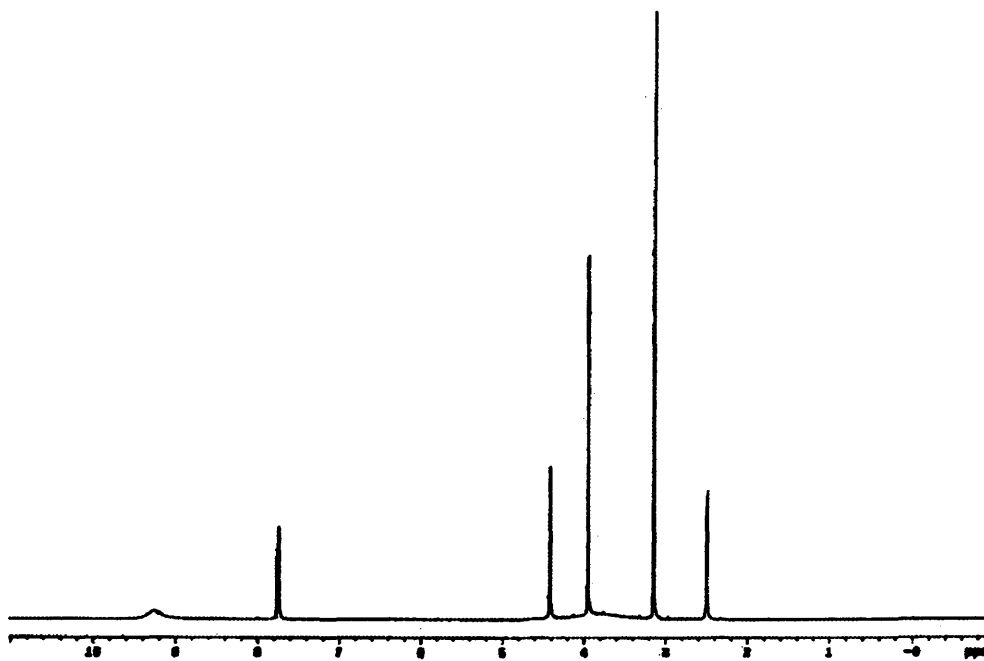
Appendix 3. ^{1}H NMR of MAMI
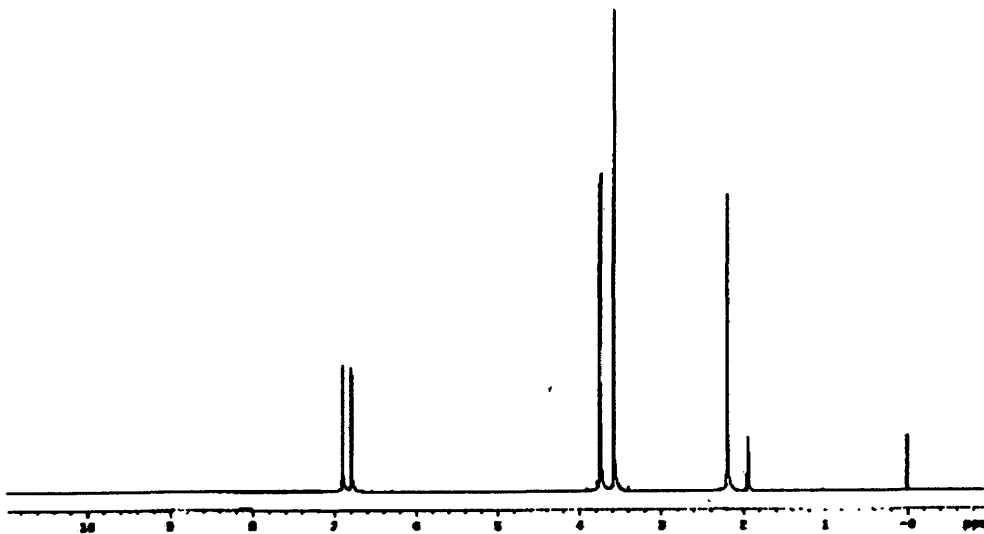
Appendix 4. ^{1}H NMR of B-MIMA
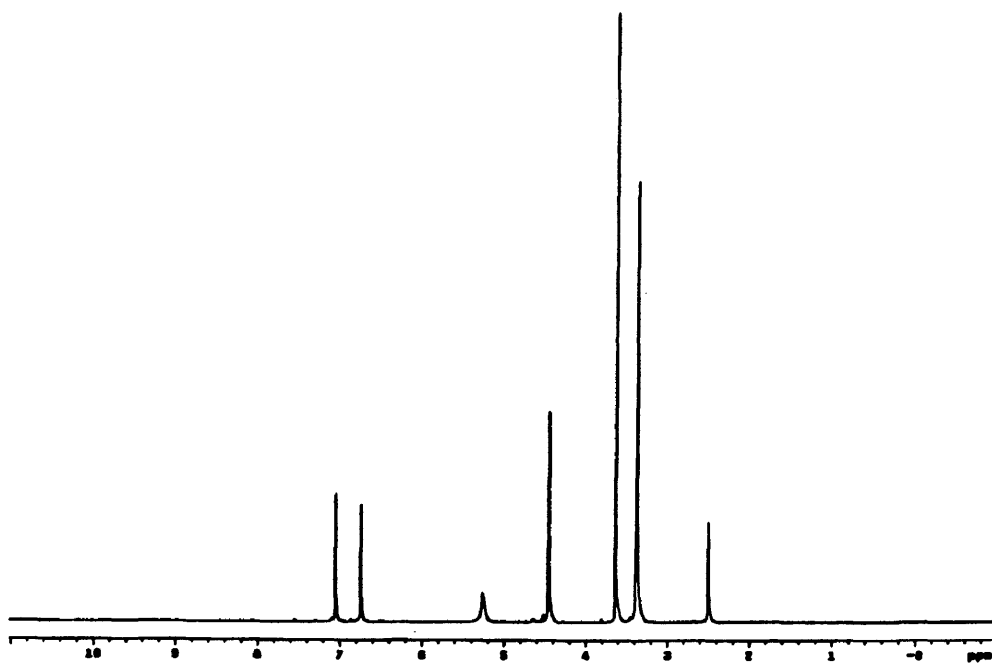
Appendix 5. ^{1}H NMR of HMMI

Appendix 6. ^{1}H NMR of CMMI
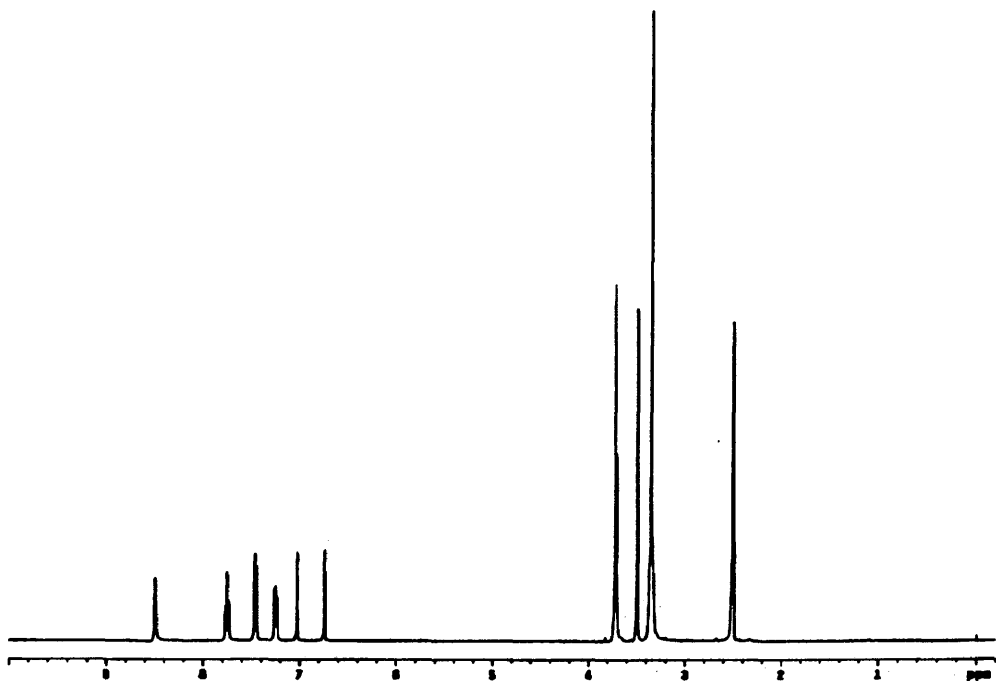
Appendix 7. ^{1}H NMR of BPIA
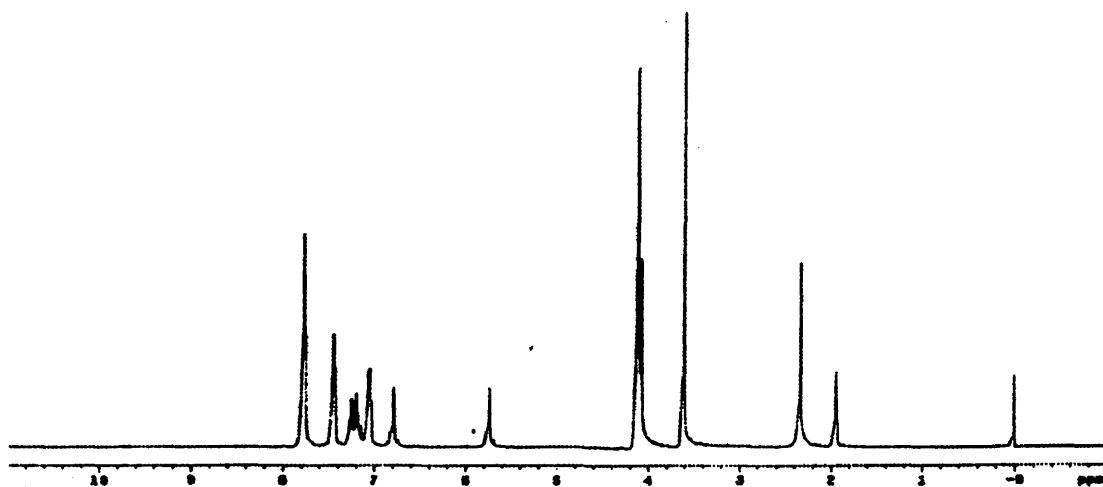
Appendix 8. ^{1}H NMR of [Hg(BPIA)$_2$](ClO$_4$)$_2$ • toluene

57
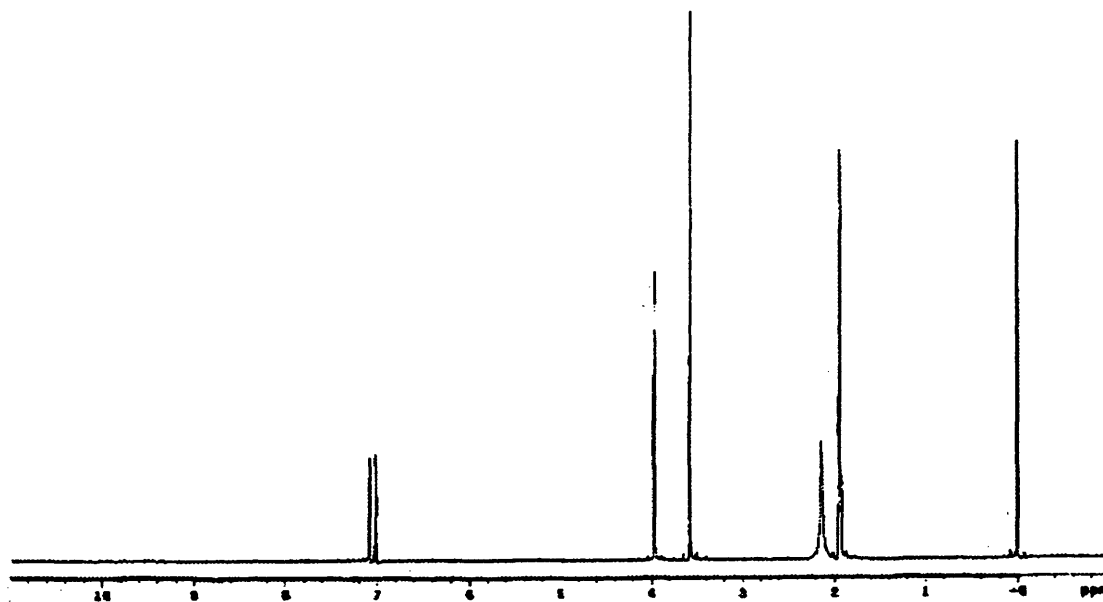
Appendix 9. ^{1}H NMR of [Hg(B-MIMA)Cl$_2$]
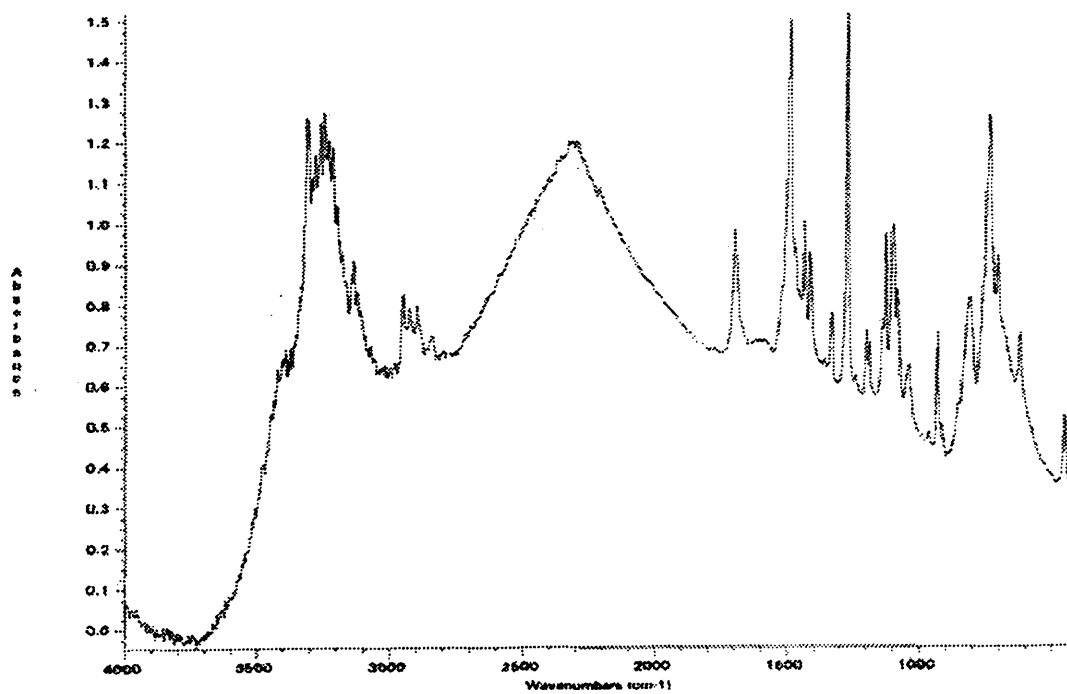
Appendix 10. IR of B-MIMA
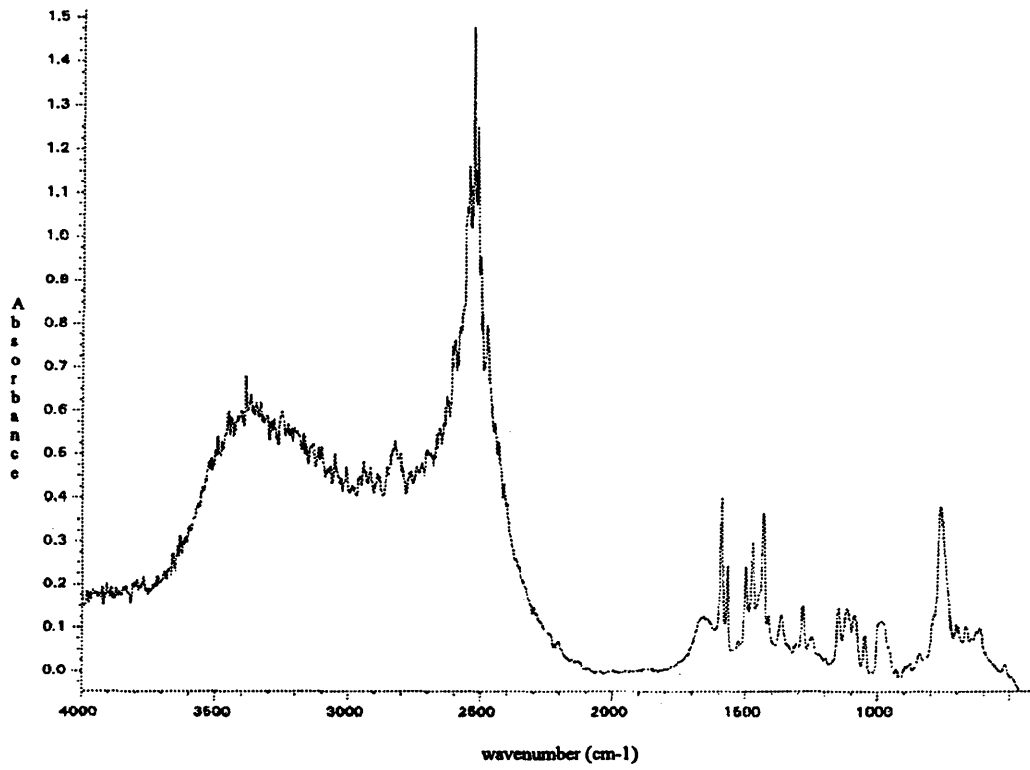
Appendix 11. IR of BPIA
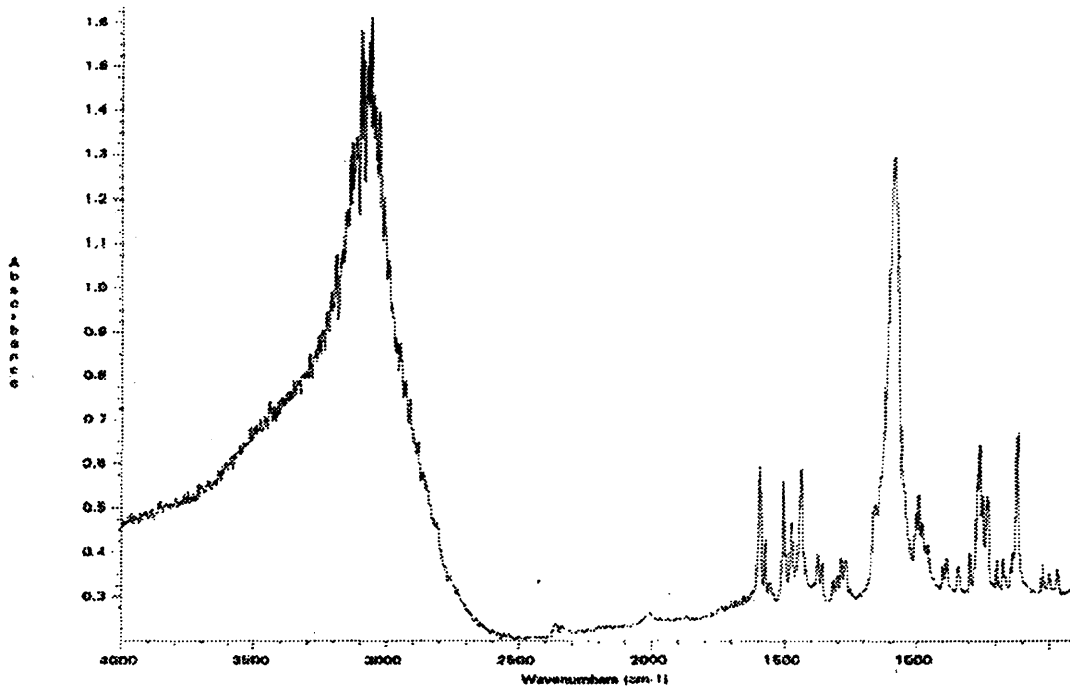
Appendix 12. IR of [Hg(BPIA)$_2$](ClO$_4$)$_2$ • toluene
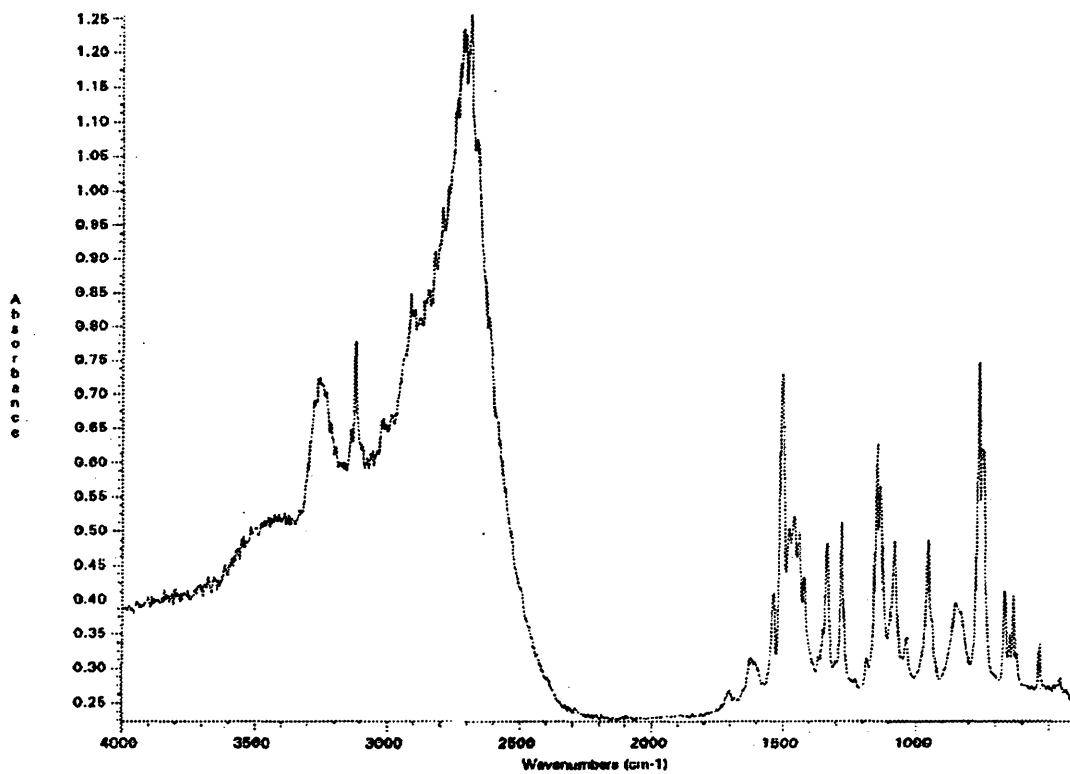
Appendix 13. IR of [Hg(B-MIMA)Cl₂]

VITA

Geoffrey S. Murphy

The author was born in Roanoke, Virginia, on January 29, 1976. He graduated from Blacksburg High School in Blacksburg, Virginia, in June of 1994, and The College of William and Mary in Williamsburg, Virginia, in May of 1998 with a B.S. degree in Chemistry.

After graduating with a M.A. degree in Chemistry, he hopes to continue his education after completing an internship in Williamsburg Community Hospital's Emergency Room.